SESCA: Predicting Circular Dichroism Spectra from Proteins Molecular Structures

Supplementary materials

Gabor Nagy[1], Maxim Igaev[1], Nykola C. Jones[2], Søren V. Hoffmann[2], Helmut Grubmüller[1]*

[1]: Department of Theoretical and Computational Biophysics, Max Planck Institute for Biophysical Chemistry, Am Fassberg 11, D-37077 Göttingen, Germany

[2]: ISA, Department of Physics & Astronomy, Aarhus University, Ny Munkegade 120, DK 8000 Aarhus C, Denmark

[*]Corresponding author

Email: hgrubmu@gwdg.de

Keywords: protein structure, CD spectrum prediction, structure validation, secondary structure

Supplementary Information:

S1 Calculation of basis spectra

The basis spectra $B_i(\lambda)$ are derived using eq. 1 independently for each available wavelength λ from a sufficiently large training set of protein structures and their CD-spectra $S_j(\lambda)$. Because typically the number of basis spectra *F* is smaller than the number of available training spectra *N* (here, *F*=1…20 and *N*=64*)*, eq. 1 represents an over-determined linear equation system. The basis spectra that minimize the average *RMSD* between calculated and measured CD spectra according to eq. 2, where $S_j^{\mathrm{calc}}(\lambda) \; = \sum_{i=1}^{F} C_{ji}\, B_i(\lambda)$, are obtained via

$$\boldsymbol{b}(\lambda) = \; (\boldsymbol{C^T}\, \boldsymbol{C})^{-1}\, \boldsymbol{C}^T\, \boldsymbol{s}(\lambda). \qquad \text{(S1)}$$

We have used matrix notation for the coefficients **C = {**C_{ij}**}** and the vector notation for the basis spectra **b**(λ)={$B_i(\lambda)$}, and CD spectra **s**(λ)={$S_j(\lambda)$}, respectively. Figures S26-S30 show basis spectrum sets that were derived by determining the basis spectra for each secondary structure (SS) element in structure classification protocol. This was done by taking the fraction of amino acids in the protein classified to be in structural element *i* as C_{ij} and applying eq. S1 on the far UV (175-269 nm) wavelength range sampled in 1 nm steps, for all 64 proteins in the TR64 set (see section 3.1).

S2 Basis set determination: the 'Hard approach'

For the hard basis set optimization approach (Fig. S1A), our aim was to find basis spectrum sets that provide the most accurate prediction of protein CD spectra. To trade-off some of the fitting accuracy for reduced overfitting, we applied a Monte Carlo (MC) approach with a cross-validation, during the search for the optimal assignments and number of basis spectra. To this aim, the protein reference set was divided into two subsets. The larger subset (training set) was used to derive the basis spectra, and the basis set accuracy was evaluated by the average *RMSD* of the calculated CD spectra of the smaller subset (evaluation set) according to eq. 2. During each optimization cycle, random changes were applied to the assignment matrix, the corresponding basis spectra for the given assignment were calculated (described in Section S1), and the new assignment was accepted or rejected based on its effect on the obtained basis set accuracy of the evaluation set ($RMSD_{\mathrm{eval}}$). At the end of the optimization, the five assignments with the lowest $RMSD_{\mathrm{eval}}$ were recorded and the complete reference set was used to fit the basis spectra and obtain the final optimized basis sets.

We imposed two constraints on the assignment factors of the hard basis sets: 1) $\sum_{i=1}^{F} \alpha_{ki} = 1$, and 2) $\alpha_{ki} \in \{1{,}0\}$. These constraints ensured that the resulting basis spectra are normalized, that there are no overlaps between the structural classes the basis spectra represent, and significantly reduced the search space of the MC algorithm. Initially, the hard optimization procedures were started from a naïve assignment (F=K) for each classification protocol, in which case **A** is the identity matrix (α_{ki} is 1 if *i*=*j* and 0 otherwise). However, the basis sets resulting from the first optimization were used as initial guesses for subsequent optimization rounds until convergence was reached both for the number of basis spectra and $RMSD_{\mathrm{eval}}$.

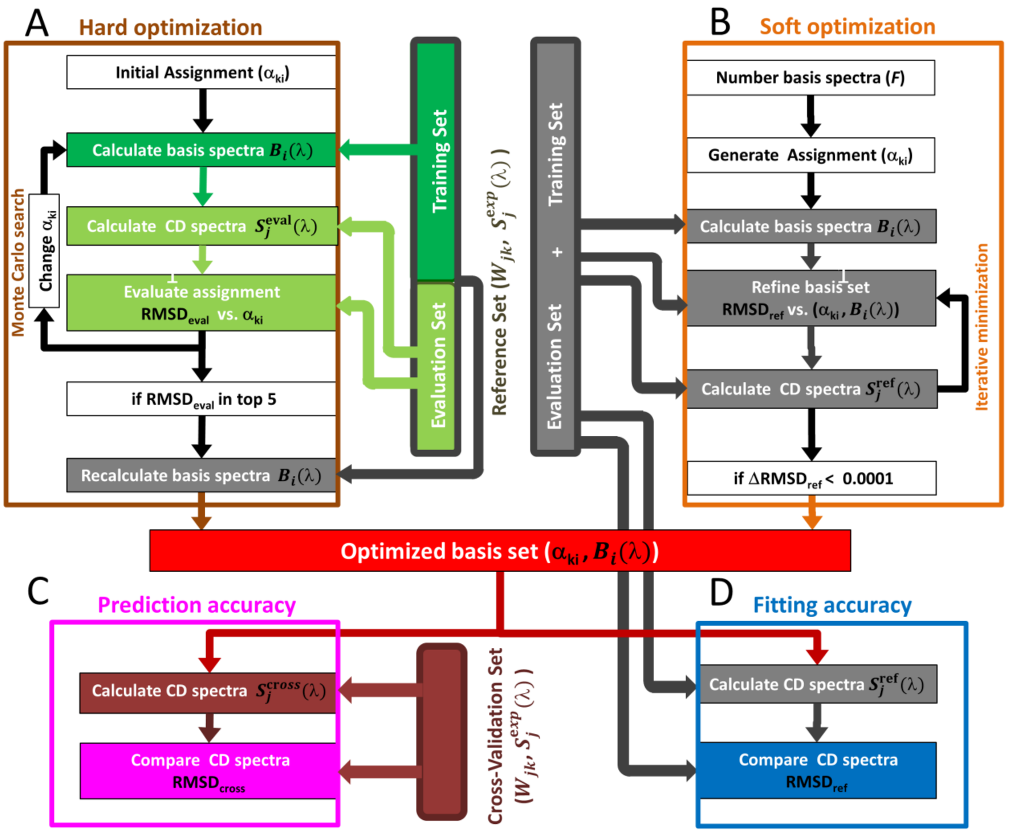
A
Hard optimization
Initial Assignment (α_{ki})
Calculate basis spectra $B_i(\lambda)$
Calculate CD spectra $S_j^{eval}(\lambda)$
Evaluate assignment
RMSD$_{eval}$ vs. α_{ki}
Change α_{ki}
Monte Carlo search
if RMSD$_{eval}$ in top 5
Recalculate basis spectra $B_i(\lambda)$
Training Set
Evaluation Set
Reference Set (W_{jk}, $S_j^{exp}(\lambda)$)
Training Set
+
Evaluation Set
B
Soft optimization
Number basis spectra (F)
Generate Assignment (α_{ki})
Calculate basis spectra $B_i(\lambda)$
Refine basis set
RMSD$_{ref}$ vs. (α_{ki}, $B_i(\lambda)$)
Calculate CD spectra $S_j^{ref}(\lambda)$
Iterative minimization
if ΔRMSD$_{ref}$ < 0.0001
Optimized basis set (α_{ki}, $B_i(\lambda)$)
C
Prediction accuracy
Calculate CD spectra $S_j^{cross}(\lambda)$
Compare CD spectra
RMSD$_{cross}$
Cross-Validation Set
(W_{jk}, $S_j^{exp}(\lambda)$)
D
Fitting accuracy
Calculate CD spectra $S_j^{ref}(\lambda)$
Compare CD spectra
RMSD$_{ref}$

Figure S1: Basis set optimization and assessment schemes. The basis sets (shown in red) are derived and optimized either though the hard or the soft optimization approach, using the same reference set of proteins, including the SS information (W_{jk}) and CD spectra ($S_j^{\text{exp}}(\lambda)$) of each protein. During the hard optimization (panel A) the reference set was divided into a training set (dark green) and an evaluation set (light green) to perform an 'internal' cross validation during the search for optimal assignments. The undivided reference set (shown as grey boxes and arrows) was used during the soft optimization (panel B) as well as at the end of the hard optimization to calculate basis spectra for the best assignments. The same undivided reference set was used to assess the fitting accuracy (panel D) of the optimized basis set (regardless of the optimization method). In contrast, during the assessment of the prediction accuracy (panel C), a different set of proteins (shown in dark red) were used for cross-validating the predictive power of the optimized basis sets.

During each hard optimization step, a random change was introduced to the assignment matrix **A**, by reassigning one of the SS elements to another structural class. Then, the basis spectra $B_i(\lambda)$ were recalculated and the average deviation ($RMSD_{\text{eval}}$) from the experimental CD spectra was computed for the evaluation set both before and after the change was applied. If $e^{-\beta*(\Delta RMSD_{eval})}$ was larger than a randomly generated number between 0 and 1, the new assignment was accepted, otherwise rejected. In the next optimization step, a new random change was applied to the last accepted assignment. The acceptance ratio in this notation was controlled by β, the strictness parameter determining how often changes with an unfavourable $\Delta RMSD_{\text{eval}}$ are accepted. By default, β = 8.0 was applied to optimizations, which was lowered (down to 1.0) if the acceptance rate in an optimization dropped below 20%. Accepted assignments with the lowest five $RMSD_{\mathrm{eval}}$ during the MC search were saved and used to calculate the basis spectra of optimized basis sets.

We note that the level of coarse graining for the SS information is given by the assignment matrix α_{ik}. Extreme cases are (a) combining all SS elements provided by the particular SS classification protocol in use into F=1 class, and (b) into F=K classes. In case (a), only very little (likely too little) information is retained – typically the α-helical content – whereas in the 'naive' case (b), the full SS information is provided with the possible risk of overfitting. Therefore, subsequent cross validation is crucial for determining the optimal level of coarse graining.

The search space for the hard optimization contains F^K possible **A** matrices, where F is the number of structural classes/basis spectra and K is the number of the SS elements. For example, assigning five structural elements to three classes defines a search space of $3^5 = 243$ assignments, whilst 19 structural elements assigned to 10 classes result in a search space of 10^{19}. When optimizing small basis sets with 5-8 SS elements, a single optimization process with 500 accepted moves was usually sufficient to completely explore the search space, often visiting the global optimum of the assignment space multiple times. In the case of more than 10 structural elements, several 10000-step optimizations were started from multiple initial assignments described below. In these cases, assignments resulting from the initial optimization procedure were used to start new parallel processes to more effectively explore the search space. To further increase the efficiency of the hard optimization, important SS elements – such as the α-helix and at least one of β-strand elements – were assigned to different classes and then excluded from being reassigned (effectively decreasing K). In addition, if the move resulted in a more favourable $RMSD_{\mathrm{eval}}$, both structural classes with no assigned SS elements and the SS elements themselves could be temporarily eliminated from the basis set. Eliminated classes and SS elements could be reintroduced to the basis set through random changes during the same optimization process, and missing SS elements were reintroduced between subsequent optimization processes to conserve the normalization of basis spectra. We have performed several optimization processes for each SS classification protocol, until the number of basis spectra in the best optimized basis sets stabilized, and $RMSD_{\mathrm{ref}}$ values similar to the soft basis sets of the same basis set size were reached (described in Section S4).

Addendum: Initial basis sets. Three deconvolution basis sets (Figs. S23-S25) were used to assess the applicability of our method without extensive optimization. The first basis set was determined by Sreerama and Woody (Set_Sreer-1) [1], contains six basis spectra (regular helix, irregular helix, regular strand, irregular strand, poly-proline helix, and disordered).). The second basis set, (Set_Perczel-1) was derived by Hollósi and Perczel [2] and contains five basis spectra (α-helix. β-strand, Turn type I/III, unordered, and other contributions). Finally, the third basis set (Set_BestSel-2) was derived for the BeStSel program by Micsonai and Kardos [3], with eight basis spectra (regular helix, irregular helix, left-handed anti-parallel, relaxed anti-parallel, and right-handed anti parallel β-strands, parallel β-strand, turn structures, and others). For each of these basis spectra, SS elements from the structure classification algorithms (DSSP and DISICL for the first two and DISICL and HbSS for the third) were assigned based on the description of the basis set in their original publications. Once the assignment was complete, the CD spectra for the proteins of the TS8, EV9, TR64 and SP175 sets were calculated using the SS content of their crystal structure and were compared to the experimental spectra.

Furthermore, we derived naive basis sets for the classification algorithms (Figs. S26-S30) DSSP (Set_DSSP-F), simplified and detailed DISICL (Set_DS-simF and Set_DS-detF, respectively), normal and extended HbSS (Set_HBSS-F and Set_HBSS-E) and the deconvolution algorithm BeStSel (Set_Bestsel-der, Fig. S31). These basis sets contained one basis spectrum for each of the algorithm's SS elements, and the SP175 data set was used as a reference set to calculate their basis spectra. These basis sets were used as initial guesses for the hard and soft optimization procedures.

S3 Calculating side-chain contributions

The individual side-chain contributions were estimated from the CD spectra of the MP79 reference set. First, the SS contributions were calculated using four optimized basis sets (DS5-4, DS-dT, DSSP-1 or DSSP-T, see the Table S8 for further details on these basis sets). Then, the resulting predicted contributions were averaged and subtracted from the rescaled (see Section 5.2) measured CD spectra. These 'secondary-structure-free' CD spectra were used in eq. S1 with the amino acid (AA) composition of the proteins and peptides as coefficients to derive one basis spectrum for each AA side chain. We also derived basis sets with more simplified representations of the side-chain contributions. These 'mixed basis sets' were derived from the MP79 reference set in three steps. First, the SS contributions were calculated and subtracted from the CD spectra. Second, basis spectra for the side chains were derived and optimized using the AA composition and the secondary-structure free CD spectra of the reference proteins. Third, the side-chain contributions were calculated and subtracted from the experimental CD spectra, and the resulting 'side-chain free' CD spectra were used to recalculate the basis spectra for the SS-dependent backbone contributions.

The optimization of the side-chain and backbone basis spectra was performed by the hard optimization scheme separately with the following modifications. Before the optimization, the MP79 reference set was separated into six subsets (each containing 13 or 14 proteins). In each optimization step, after the SS elements / AAs were grouped and assigned to basis spectra, one of the MP79 subsets was designated as the evaluation set, whilst the rest of the reference proteins were used to derive the basis spectra (as a training set). The derived basis spectra were used to calculate the CD spectra of the evaluation set. This process was repeated six times such that each of the subsets was predicted once from the rest of the MP79 reference set. After calculating each of the evaluation subsets, their *RMSD* was averaged and used as $RMSD_{\mathrm{eval}}$ to determine if the assignment is accepted or rejected. The optimization process was continued until 250 - 5000 accepted moves were reached (depending on the basis set size), with the five best assignments recorded for further use. Basis spectra for the recorded assignments were recalculated from the full MP79 reference set. These finalized basis spectra were used to predict the 'secondary-structure free' or 'side-chain free' CD spectra of the TS8 protein set as cross validation. The combination of side-chain and backbone basis spectra that predicted the TS8 protein set with lowest $RMSD_{\mathrm{cross}}$ were combined into mixed basis sets. Then, mixed basis sets were used to calculate the CD spectra of the SP175, GXG20, GP59, and TS8 data sets, so that they can be compared with the SS-only optimized basis sets, and predictions from PDB2CD and DichroCalc. We note that the measured CD spectra of the GXG peptides were normalized for the number of amino acids (three) as usual, but they were not rescaled based on the predicted spectra from backbone-only basis sets. The scaling factors were omitted because the GXG spectra were mostly determined by their side chain contributions these basis sets still lacked.

S4 Basis set determination: The ‘soft approach’

The hard optimization scheme introduced above is limited to a restricted assignment factor space ($\alpha_{ki} \in \{0,1\}$) and, therefore, it should be possible to further improve the accuracy of reconstructing the CD spectra from the SS information by removing this limitation. Accordingly, in our more general soft optimization approach, the assignment factors can be any real number ($\alpha_{ki} \in R$). During the soft optimization, we simultaneously derived the basis spectra and assignment factors that most accurately reproduced the CD spectra of the reference protein data set (best fitting accuracy). Consequently, besides the spectral and structural information of the reference data set, only the desired number of basis spectra is specified for the soft optimization, and no ‘internal’ cross-validation is required to trade-off the accuracy of the fit for an improved general predictive power. To obtain the optimal basis sets, the non-linear equation system defined by eq. 4 has to be solved simultaneously for all wavelengths of each protein spectrum in the reference data set. In matrix notation, this optimization problem is

$$\left|\left|\boldsymbol{W}\,\boldsymbol{A}\,\boldsymbol{B}-\boldsymbol{S}\right|\right|^{2}\overset{!}{=}\mathrm{min}, \qquad \text{(S2)}$$

where **S**=$\{S_{jl}\}$ and **W**=$\{W_{jk}\}$ are the matrices containing the spectral and structural information of the reference set, respectively, and the matrix **B** =$\{B_{il}\}$ describes the basis spectra. The matrix elements S_{jl} and B_{il} are obtained by discretizing the experimental CD spectra $S_j(\lambda)$ and basis spectra $B_i(\lambda)$ at L wavelengths. This optimization problem is solved simultaneously for the matrices **A** and **B** by setting their element-wise matrix derivatives to zero:

$$\frac{\partial}{\partial \boldsymbol{A}}\mathrm{tr}[(\boldsymbol{W}\,\boldsymbol{A}\,\boldsymbol{B}-\boldsymbol{S})^{\boldsymbol{T}}\ (\boldsymbol{W}\,\boldsymbol{A}\,\boldsymbol{B}-\boldsymbol{S})] =$$

$$2\,\boldsymbol{B}\,\boldsymbol{B}^{\mathbf{T}}\,\boldsymbol{A}^{\mathbf{T}}\,\boldsymbol{W}^{\mathbf{T}}\,\boldsymbol{W}-2\,\boldsymbol{B}\,\boldsymbol{S}^{\mathbf{T}}\,\boldsymbol{W}\ \overset{!}{=}\ 0 \qquad \text{(S3)}$$

$$\frac{\partial}{\partial \boldsymbol{B}}\mathrm{tr}[(\boldsymbol{W}\,\boldsymbol{A}\,\boldsymbol{B}-\boldsymbol{S})^{T}\ (\boldsymbol{W}\,\boldsymbol{A}\,\boldsymbol{B}-\boldsymbol{S})] =$$

$$2\,\boldsymbol{B}^{\mathbf{T}}\,\boldsymbol{A}^{\mathbf{T}}\,\boldsymbol{W}^{\mathbf{T}}\,\boldsymbol{W}\,\boldsymbol{A}-2\,\boldsymbol{S}^{\mathbf{T}}\,\boldsymbol{W}\,\boldsymbol{A}\ \overset{!}{=}0 \qquad \text{(S4)}$$

which, yields two coupled non-linear matrix equations

$$\boldsymbol{A}=(\boldsymbol{W}^{\mathbf{T}}\,\boldsymbol{W})^{-\mathbf{1}}\,\boldsymbol{W}^{\mathbf{T}}\,\boldsymbol{S}\,\boldsymbol{B}^{\mathbf{T}}\,(\boldsymbol{B}^{\mathbf{T}}\,\boldsymbol{B})^{-\mathbf{1}} \qquad \text{(S5)}$$

and

$$\boldsymbol{B}=\ (\boldsymbol{A}^{\mathbf{T}}\,\boldsymbol{W}^{\mathbf{T}}\,\boldsymbol{W}\,\boldsymbol{A})^{-\mathbf{1}}\,\boldsymbol{A}^{\mathbf{T}}\,\boldsymbol{W}^{\mathbf{T}}\,\boldsymbol{S} \qquad \text{(S6)}$$

Equations S5 and S6 are solved iteratively, starting from a random generated matrix **A** ($0.0 \leq \alpha_{ki} \leq 1.0$) to obtain an initial **B** via eq. S6, which is inserted into eq. S5 to obtain an improved **A**, repeated until convergence. A summary of the soft optimization scheme is shown in Fig. S1. This soft optimization procedure was systematically repeated for each SS classification protocol K times to obtain optimized basis sets with 1-K basis spectra (K being the number of SS elements in the classification protocol). These series of basis sets determine the best fitting accuracy as the function basis set size and SS classification. For each optimization procedure, the convergence criterion was to reach less than $\Delta RMSD_{\mathrm{fit}}$ = 0.0001 x 10^3 deg cm^2/dmol change between iterations.

Finally, we note that the hard combination of SS elements is a special case of the more general soft combination approach and therefore, one might expect the latter to yield more accurate calculated spectra for the reference proteins from the same amount of structural information. Because in the soft optimization approach the assignment factors α_{ki} can adopt any real number without further constraints, eq. 3 yields linear combinations of the SS fractions W_{kj}. Hence, each basis spectrum $B_i(\lambda)$ can be understood as a 'collective' SS class, such as '0.3 α-helical + 0.7 β-sheet'. Of course, the collective SS classes introduce another layer of complexity to the optimization problem, and therefore increase the chances of overfitting the basis spectra.

S5 The analysis of spectral components

The overall accuracy of our method is limited by two factors, first, the information content of the SS composition, and second, the applicability of linear combinations of basis spectra in approximating the experimental CD spectra. The first factor was addressed by our soft optimization approach (Section S4). The second factor determines an upper limit for the fitting accuracy (lowest $RMSD_{\mathrm{fit}}$) given a set of reference CD spectra and the number of basis spectra used. To this end, we carried out a principal component analysis (PCA) on CD spectra of the SP175 reference set (see Section 3.1). PCA is a mathematical method to describe a (multidimensional) data set of N members by a basis set of N orthogonal principal component (PC) vectors. How much the data points differ from the average of the set (the variance of the data set) along a PC vector is quantified by its eigenvalue. It is possible to describe a data set with just a few (*F*) PC vectors of the highest eigenvalues (dimensionality reduction)[32], which – by construction – retains the maximum possible variance of the data set, and consequently, provides the reconstruction with the smallest possible deviation. Here, we used PCA to describe the reference CD spectra (a set of *L* dimensional data points) by basis sets constructed from 1-10 PC vectors of the highest eigenvalues. The basis spectrum coefficients (C_{ij}) of the protein *j* for these basis sets were defined as the projection of the CD spectrum along the particular PC vector *i* (described below). Note that this analysis is based solely on CD spectra of the reference data set, and does not account for any possible source of inaccuracy related to structure, SS calculations, or scaling errors within the reference set.

During the reconstruction, the PC vectors obtained from PCA were described by the matrix $\mathbf{V}=\{V_{pl}\}$, where the indices *p* (1….P) and *l* (1….L) stand for the principal component (in order of their eigenvalue) and wavelength, respectively. In our case, each $\mathbf{v}_{\mathbf{r}\mathrm{p}}$ row vector of the matrix **V** is one of the discretized PC vectors. The spectra of a reference protein data set were reconstructed using the first P={1-10} principal components

$$S_{jl} = S_l^{ave} + \sum_{p=1}^{P} C_{jp}\, V_{pl}, \qquad \text{(S7)}$$

where S_{jl} is the circular dichroism of the j^{th} reconstructed protein spectrum at the wavelength l, C_{jp} is the projection of that spectrum along the PC vector p, V_{pl} and S_l^{ave} are the value of the PC vector and the average CD signal of the data set at wavelength l, respectively. The projection of spectrum j along the principal component p can be calculated by taking the scalar product of the normalized spectrum and the PC vector

$$C_{jp} = (\boldsymbol{s}_{rj} - \boldsymbol{s}^{ave})^T\ \boldsymbol{v}_{rp}. \qquad \text{(S8)}$$

The vector $\boldsymbol{s}^{\mathrm{ave}} = \{S_l^{\mathrm{ave}}\}$ is the averaged CD spectrum of the data set.

The projections along the PC vectors are analogous to the basis spectrum coefficients. Therefore, Pearson correlation (R_{pearson}) between the SS composition, AA composition, and the projections were calculated for the proteins in the SP175 reference set to estimate the importance of these structural descriptors in calculating the CD spectra. The Pearson correlation between these descriptors were calculated according to

$$R_{\mathrm{pearson}} = \frac{\sum(X_j - \bar{X})\cdot(Y_j - \bar{Y})}{\sqrt{\sum(X_j - \bar{X})^2}\cdot\sqrt{\sum(Y_j - \bar{Y})^2}}, \qquad \text{(S9)}$$

where X_j and Y_j are either the fraction of an AA, the fraction of residues classified as a SS element, or the projection of the CD spectrum along a principal component for the protein j, whilst $\bar{X}$ and $\bar{Y}$are the calculated averages for the whole reference set.

S6 Describing the error of CD spectrum predictions

Here, we separate the errors of our CD spectrum predictions into an error term that depends on the SS composition of the underlying protein structural model (SS-dependent error), and an SS-independent error term that results from inaccuracies of the prediction method itself. This separation allows us to determine the typical prediction error of SESCA basis sets, and to estimate the error of the underlying structural model based on the accuracy of its predicted CD spectrum.

To this end, we assume that the true SS composition of the solution structure is described by the coefficients C_{ji}^0. The CD spectrum predicted from this correct composition deviates slightly from the experimental spectrum (quantified by $RMSD_j^0$), due to inaccuracies in our basis spectra (B_{il}), unaccounted contributions to the CD spectrum (e.g. from co-factors and side chains), and potential measurement errors of the spectrum itself. After accounting for all the errors independent of the SS composition at every wavelength (ΔS_{jl}) the experimentally measured CD spectrum is expressed as

$$S_{jl}^{\mathrm{exp}} = \sum_{i=1}^{F} C_{ji}^{0} \cdot B_{il} + \mathit{\Delta} S_{jl}. \qquad \text{(S10)}$$

If we predict the measured CD spectrum from a structural model with the SS composition C_{ji}, the *RMSD* of the predicted spectrum ($S_{jl}^{\mathrm{calc}} = \sum_{i=1}^{F} C_{ji} \cdot B_{il}$) will be

$$RMSD_j = \sqrt{\frac{\sum_{l=1}^{L} \left(S_{jl}^{\mathrm{exp}} - S_{jl}^{\mathrm{calc}}\right)^2}{L}} = \sqrt{\frac{\sum_{l=1}^{L} \left(M_{jl} + \mathit{\Delta} S_{jl}\right)^2}{L}}, \qquad \text{(S11)}$$

where $M_{jl} = \sum_{i=1}^{F} \mathit{\Delta} C_{ji} \cdot B_{il}$ describes the SS-dependent error of the predicted spectrum at wavelength *l*, $\mathit{\Delta} C_{ji} = C_{ji}^{0} - C_{ji}$ is the structural model's error in the coefficient of SS-class *i*, and B_{il} is the CD intensity of for the basis spectrum of SS-class *i* at wavelength *l*.

Equation S11 can be rewritten using vector notation, considering the total error of the predicted spectrum for protein *j* at each wavelength *l* to be described by the vector $\vec{\boldsymbol{R}} = \vec{\boldsymbol{M}} + \vec{\boldsymbol{S}}$. Here, $\vec{\boldsymbol{M}} = \left\{M_{j1};\ M_{j2}; \dots\ M_{jL}\right\}$ is the wavelength vector containing SS-dependent error terms, whereas $\vec{\boldsymbol{S}} = \left\{\mathit{\Delta} S_{j1};\ \mathit{\Delta} S_{j2}; \dots\ \mathit{\Delta} S_{jL}\right\}$ is the wavelength vector of the SS-independent error terms for protein *j*, respectively. We note that the lengths of these vectors are connected via $\left|\vec{\boldsymbol{R}}\right|^2 = \left|\vec{\boldsymbol{M}}\right|^2 + \left|\vec{\boldsymbol{S}}\right|^2 + 2 \cdot \left|\vec{\boldsymbol{M}}\right| \cdot \left|\vec{\boldsymbol{S}}\right| \cdot \cos\varphi$, where $\cos\varphi$ is the angle between the vectors $\vec{\boldsymbol{M}}$ and $\vec{\boldsymbol{S}}$. Because $RMSD_j$ is the average root-mean-squared deviation from the measured spectrum, $RMSD_j{}^2 = \frac{1}{L} \cdot \left|\vec{\boldsymbol{R}}\right|^2$. Combining these two equations, $RMSD_j$ is written as

$$RMSD_j{}^2 = M_j{}^2 + RMSD_j^{0\,2} + 2 \cdot M_j \cdot RMSD_j^{0} \cdot \cos\varphi, \qquad \text{(S12)}$$

where $M_j = \frac{|\vec{\boldsymbol{M}}|}{\sqrt{L}} = \sqrt{\frac{\sum_{l=1}^{L} M_{jl}{}^2}{L}}$ is the average SS-dependent error, and $RMSD_j^{0} = \frac{|\vec{\boldsymbol{S}}|}{\sqrt{L}} = \sqrt{\frac{\sum_{l=1}^{L} \Delta S_{jl}{}^2}{L}}$ is the average SS-independent error. We also note that $RMSD_j^{0}$ is equal to the RMSD of the spectrum predicted from the correct SS composition (C_{ji}^{0}).

Equation S12 allows us to separate the SS-dependent error from the SS-independent error, and to quantify the error in the SS composition of any protein model based on $RMSD_j$ of its predicted spectrum. To this end, we introduce the total error in the model's secondary structure composition as $\varDelta SS_j = \sum_{i=1}^{F} \left|\varDelta C_{ji}\right|/2$, which is equal to the (minimum) fraction of residues in the protein model with incorrect SS classification. We note that any misclassified residue in the model causes a positive (in its current class) and a negative (in its supposed class) error in the coefficients, and thus, the sum of $\left|\varDelta C_{ji}\right|$ was divided by two to obtain $\varDelta SS_j$. The SS-dependent error at wavelength l can be written as $M_{jl} = \left(\sum_{i=1}^{F} \frac{\varDelta C_{ji} \cdot B_{il}}{\varDelta SS_j}\right) \cdot \varDelta SS_j$, where $\varDelta SS_j$ gives the magnitude of the structural model's error, and the ratios $\frac{\varDelta C_{ji}}{\varDelta SS_j}$ describe how $\varDelta SS_j$ is distributed between the coefficients of the SS classes. This allows one to express the proportionality between the SS-dependent error and the total model error as

$$M_j = \left(\sqrt{\frac{1}{L} \cdot \sum_{l=1}^{L} \left(\sum_{i=1}^{F} \frac{\varDelta C_{ji} \cdot B_{il}}{\varDelta SS_j}\right)^2}\right) \cdot \varDelta SS_j = m_j \cdot \varDelta SS_j \ . \qquad \text{(S13)}$$

Note that, for all structural models with the same $\frac{\varDelta C_{ji}}{\varDelta SS_j}$ ratios, the SS-dependent error will be a linear function of $\varDelta SS_j$. Combining eqs. S12 and S13 results in a second order equation which can be solved for $\varDelta SS_j$ to express the error in the structural model

$$\varDelta SS_j = \frac{\sqrt{RMSD_j{}^2 + RMSD_j^{0\,2} \cdot (\cos^2 \varphi - 1)}}{m_j} - \frac{RMSD_j^0 \cdot \cos \varphi}{m_j}. \qquad \text{(S15)}$$

Equation S15 shows that, for a given m_j, $RMSD_j$, and $RMSD_j^0$ value $\varDelta SS_j$ will be the largest if the two error vectors are anti-parallel ($\cos \varphi = -1$), in which case $\varDelta SS_j = \left(RMSD_j + RMSD_j^0\right)/m_j$, and smallest if the error vectors are parallel ($\cos \varphi = 1$), resulting in $\varDelta SS_j = \left(RMSD_j - RMSD_j^0\right)/m_j$. However, if the SS-independent error contains only random noise and no systematic errors, the two error terms should be statistically independent and $\cos \varphi \approx 0$. In this case, eq. S15 is simplified to $\varDelta SS_j = \sqrt{RMSD_j{}^2 - RMSD_j^{0\,2}}/m_j$, which approaches a linear function $\varDelta SS_j = RMSD_j/m_j$ for $RMSD_j{}^2 \gg RMSD_j^{0\,2}$.

The obtained equations for the three special cases ($\cos \varphi = \{0, +1, -1\}$ will be used in Section S8 to determine the best estimate for $\varDelta SS_j$ assuming that the SS-dependent and SS-independent errors of the predicted spectrum are statistically independent ($\cos \varphi = 0$), but providing the upper and lower bounds for the total model error if the assumption is incorrect.

S7 CD spectrum deconvolution

Spectrum deconvolution is a method to decompose a measured CD spectrum of a target protein into a linear combination of basis spectra (see eq. 1 in the main text). This procedure is often used to determine the SS composition (C_{ji}) that best describes the solution structure of a target protein. For a given set of basis spectra (B_{il}), the SS composition that fits the spectrum best minimizes the average deviation (*RMSD*$_j$) between the decomposed ($S_{jl}^{dec} = \sum_{i=1}^{F} C_{ji} \cdot B_{il}$) and the measured spectrum ($S_{jl}^{\exp}$). Therefore, to find the optimal C_{ji} we minimized the function

$$F\left(C_{ji}\right) = \sqrt{\frac{1}{L}\sum_{l=1}^{L}\left(S_{jl}^{\exp} - \sum_{i=1}^{F} C_{ji}\cdot B_{il}\right)^2} + \Lambda_1 \cdot \left|1 - \sum_{i=1}^{F} C_{ji}\right| + \Lambda_2 \cdot \sum_{i=1}^{F} \delta(C_{ji}), \tag{S16}$$

where the first term is the *RMSD* of the decomposed spectrum, whilst the second and third terms ensure that C_{ji} add up to 1 and remain positive, respectively. Note that Λ_1 and Λ_2 are constant Lagrange multipliers in this equation, whereas the function $\delta\left(C_{ji}\right) = -C_{ji}$ if the coefficient is negative and 0 otherwise.
Our minimizations were carried out using an adaptive simplex minimizer (Nelder-Mead) [4] algorithm from the scientific python package. The minimizations were continued until 5000 iterations or until the convergence criterion $\Delta F\left(C_{ji}\right) < 10^{-15}$ was reached. To find the global *RMSD* minimum of our reference proteins, first 10 minimizations were started from random initial SS compositions, and minimization result with the lowest *RMSD* was taken. If none of minimizations reached convergence for a protein, a second round of 50 minimizations with 50 000 iterations were launched. If still no minimum was found, then a single, 50 000 step minimization was started from the SS composition of the proteins crystal structure, and the SS composition with the lowest *RMSD* found was used as the best one.

S8 Deriving error models for structure validation

Here, we provide and test error models that estimate the total error (ΔSS_j) in the SS composition (C_{ji}) of a protein structural model based on the error (*RMSD*$_j$) of its predicted CD spectrum. The equations described in Section S6 allow one to exactly calculate ΔSS_j from $RMSD_j$, provided that we know the parameters m_j, $RMSD_j^0$, and cos φ. In summary, m_j is the slope that connects the average SS-dependent error (M_j) of the predicted spectrum with the error of the structural model ΔSS_j, $RMSD_j^0$ describes the average SS-independent error of the predicted spectrum, and cos φ describes the non-additivity between the two error terms.

Unfortunately to calculate these parameters, knowing the correct SS composition (C_{ji}^0) of protein j under the conditions CD spectrum (which is used for validating the structural model) was measured is essential. Because C_{ji}^0 is typically unknown, we determine average parameters that allow the estimation of ΔSS_j as accurately as possible.

To determine the best ΔSS_j estimation method we 1) approximate C_{ji}^0 and $RMSD_j^0$ for each reference protein of the SP175 set by spectrum deconvolution (see Section S7), 2) compute $RMSD_j$ and ΔSS_j (compared to C_{ji}^0) for each reference structure in the SP175 set using several basis sets, 3) fit the parameters for the ΔSS_j estimation (described below) to the obtained $RMSD_j$ and ΔSS_j values, 4) evaluate the error models by comparing the estimated ΔSS_j to the ΔSS_j obtained from deconvolution, and 5) determine the error margins for our estimated ΔSS_j values.

We note that if the measured CD spectrum and the basis set contain no severe systematic errors, $RMSD_j^0$ is the minimum of the *RMSD*(C_{ji}) landscape. In the deconvolution algorithm described in Section S7 we approximate C_{ji}^0 and $RMSD_j^0$ for the SP175 reference proteins by minimizing $RMSD_j$ as function of C_{ji}. We used the differences between the approximated C_{ji}^0 and

C_{ji} of the reference structures to compute ΔSS_j for the SP175 proteins, and after predicting the reference spectra from C_{ji}, to obtain 71 $RMSD_j$ vs. ΔSS_j values for several basis sets.

For each of these basis sets the resulting data points in $RMSD_j{}^2$ vs. $\Delta SS_j{}^2$ space were fitted with three equations given in the Fig. S2 (bottom) using orthogonal distance regression [5] (ODR). These equations – derived from eq. S15 (Section S6) using different assumptions – yielded similar fit parameters within the estimated uncertainties (σ_m, σ_R), including a fitted value of $\cos\varphi_f$ = 0±10^{-5} for equation C, which resulted in eqs. B and C giving virtually identical solutions for all tested basis sets. For simplicity, in the table in Fig. S2 we only show fit parameters obtained from eq. B for each basis set, and used for our final error model.

Next, as illustrated in Fig S2 (left) for the DS-dT basis set, we compare the estimated $\Delta SS_j^{\mathrm{est}}$ values (solid colored lines) with the correct ΔSS_j values (black cross symbols) to determine the best estimate. To quantify the goodness of the fits, we computed $\chi^2 = \sum_{j=1}^{N}\left(\Delta SS_j{}^2 - \Delta SS_j^{\mathrm{est}2}\right)^2/(N-P)$, where N=71 is the number of reference proteins, and P={1,2,3} is the number of fit parameters for eqs. A, B, and C, respectively. The obtained average χ^2 values indicate that eq. A describes the SP175 reference set slightly better than eqs. B and C do. Additionally, eqs. B and C do not yield real solutions ΔSS_j^{est} for $RMSD_j < R_f$, in which cases $\Delta SS_j^{est} = 0$ is assumed. This limitation further increases the average deviation between the real and estimated ΔSS_j as shown by the tabulated $\Delta\Delta SS = \sqrt{\frac{1}{N}\sum_{j=1}^{N}(\Delta SS_j - \Delta SS_j^{\mathrm{est}})^2}$ values in Fig. S2. Therefore, we chose the best estimate to be $\Delta SS_j^{est} = RMSD_j\,/m_f$ for our error models.

Finally, we defined two error margins for ΔSS_j^{est}. The more narrow error margin (purple dashed line) is defined by the average error of the best estimate as $\Delta SS_j^{est} \pm \Delta\Delta SS$, and contains 73% of the data points on average. The broader error margin (green dashed line) is defined based on eq. S15, assuming the fitted average m_j and $RMSD_j^0$ parameters (m_f and R_f, respectively), and strong correlations between the error terms ($\cos\varphi = \pm 1$). In this case the upper and lower bounds of $\Delta SS_j^{\mathrm{est}}$ are $\Delta SS_j^{\mathrm{up}} = \left(RMSD_j + (R_f + \sigma_R)\right)/\left(m_f - \sigma_m\right)$ and $\Delta SS_j^{\mathrm{low}} = \left(RMSD_j - (R_f + \sigma_R)\right)/\left(m_f + \sigma_m\right)$, and contain ~94% of reference proteins on average.

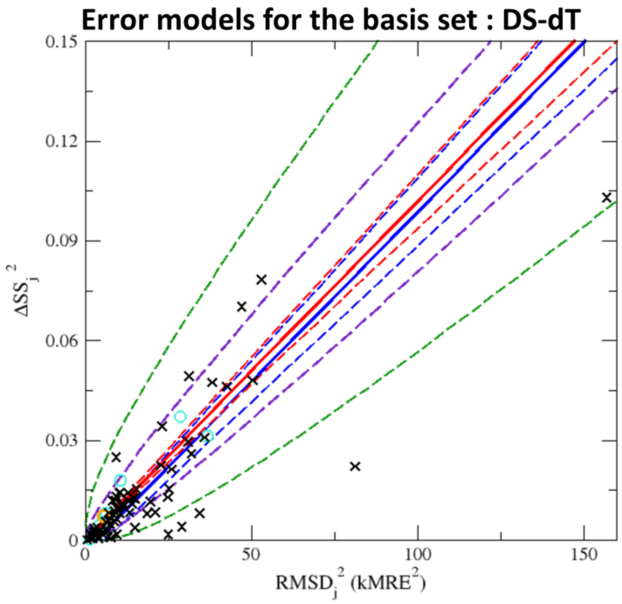

Fit Summary

Basis set	DS-dT	DSSP-1	HBSS-3	DS5-4	Average
m_f (kMRE)	31.3	18.2	17.3	15.3	21.0
σ_m (kMRE)	1.3	2.0	1.0	1.8	1.5
R_f (kMRE)	1.79	1.08	0.99	2.25	1.52
σ_R (kMRE)	0.54	0.34	1.40	0.75	0.76
χ^2-A (10^{-4})	12.67	19.35	15.99	19.65	16.91
χ^2-B (10^{-4})	12.59	19.50	16.20	19.62	16.98
χ^2-C (10^{-4})	12.78	19.79	16.44	19.91	17.23
$\Delta\Delta$SS-A (%)	2.6	5.4	6.3	7.9	5.5
$\Delta\Delta$SS-B (%)	2.97	5.61	6.62	9.74	6.2
$\Delta\Delta$SS-C (%)	2.97	5.61	6.62	9.74	6.2
Bounds (%)	74.6	70.4	81.7	64.8	72.9
Bounds (%)	94.4	90.1	90.1	100	93.7

Fit Equations:	Assumptions:
Estimate A: $\Delta SS_j{}^2 = RMSD_j{}^2/m_f{}^2$	$\cos\Theta = 0,\ R_f \ll RMSD_j$
Estimate B: $\Delta SS_j{}^2 = (RMSD_j{}^2 - R_f{}^2)/m_f{}^2$	$\cos\Theta = 0$
Estimate C: $\Delta SS_j{}^2 = \left(\sqrt{RMSD_j{}^2 + R_f{}^2 \cdot (\cos\Theta^2 - 1)} - R_f \cdot \cos\Theta\right)^2 /m_f{}^2$	none

Figure S2: Comparison between three different estimates for the total error in the SS composition (ΔSS_j) of protein structural models. The estimation of ΔSS_j is based on the deviation ($RMSD_j$) between the measured CD spectrum and spectrum predicted from the structural model. The error estimates (A-C) with three functional forms (at the bottom) were fitted to the SP175 reference proteins shown as black cross symbols on the left side of the figure. The best estimates (shown as solid lines) with estimated error margins (shown as dashed lines, see section S8) are also displayed for the DS-dT basis set. Obtained fit parameters ($m_f, \sigma_m, R_f, \sigma_R$), goodness of fit measures ($\chi^2, \Delta\Delta SS$) and the percentage of data points contained within the selected error margins (Bounds) for four tested basis sets (DS-dT, DSSP-1, HBSS-3, DS5-4) are listed in the table (to the right).

S9 Determining the difficulty of CD spectrum predictions

To quantify the difficulty of predicting the CD spectrum of each reference protein j in our data sets (SP175 and TS8) from its structural model, we computed the mean error of CD spectrum predictions ($RMSD_j^{\mathrm{mean}}$) for protein each j. As described in Section 3.6, $RMSD_j^{\mathrm{mean}}$ were determined by calculating CD spectra using six different prediction methods and averaging the deviations between the measured CD spectrum and the predicted spectra at every wavelength. We also determined the normal range of $RMSD_j^{\mathrm{mean}}$ by calculating the average ($RMSD_{\mathrm{set}}^{\mathrm{mean}}$) and standard deviation of theses values scatter (σ_{set}) for our reference sets. We found that these values were similar for the SP175 ($RMSD_{\mathrm{fit}}^{\mathrm{mean}}$ = 3.3 kMRE, σ_{fit}= 1.1 kMRE) and TS8 data sets ($RMSD_{\mathrm{cross}}^{\mathrm{mean}}$ = 3.2 kMRE, σ_{cross}=1.3 kMRE). As shown in Fig. S3A, we considered proteins as outliers, and therefore, particularly difficult to predict, if their $RMSD_j^{\mathrm{mean}}$ value was larger than $RMSD_{\mathrm{cross}}^{\mathrm{mean}} + \sigma_{\mathrm{cross}}^{\mathrm{mean}}$ = 4.5 kMRE.

Next, we tested if the large $RMSD_j^{\mathrm{mean}}$ values of the outliers – listed in Fig. S3B – can be explained based on two potential sources of error, namely inaccuracy of the used structural models, and the inaccurate normalization of the measured spectrum intensities (identified in Sections 5.1 and 5.2, respectively).

First we accounted for the inaccurate normalization of the reference CD spectra by rescaling the intensities to match the intensity of the predictions (see Section 5.2). Scaling the measured spectra decreased the mean *RMSD* of the outlier proteins (henceforth the OP13 set) significantly from 6.2 kMRE to 3.6 kMRE), but also decreased $RMSD_{\mathrm{cross}}^{\mathrm{mean}}$ to 2.7 kMRE, and σ_{cross} to 0.7 kMRE, thus lowering the threshold of what is considered an outlier to 3.4 kMRE. Despite the lower *RMSD* threshold, intensity scaling reduced $RMSD_j^{\mathrm{mean}}$ for five of the thirteen proteins (colored blue in Fig. S3) by so much that they were no longer considered as outliers, including the reference protein with the largest *RMSD*; Subtilisin Carlsberg (SP175/67, spectra shown in Fig. S3C). Then, the rescaled CD spectra were subjected to deconvolution using the four SESCA basis sets (Section 3.6) to estimate and account for errors in the SS composition ($\Delta SS_j^{\mathrm{mean}}$) of the reference structures. Calculating the CD spectra from the ideal SS composition further reduced both $RMSD_{\mathrm{OP13}}^{\mathrm{mean}}$ to 2.1 kMRE and the threshold *RMSD* to 2.0 kMRE. In addition, it indicated that for two outliers (in magenta) – Avidin (SP175/8) and Glutamate dehydrogenase (SP175/34) – the above average $RMSD_j^{\mathrm{mean}}$ is due to the combination of inaccurate spectrum normalization and model inaccuracies.

For the remaining six outlier proteins (in red) $RMSD_j^{\mathrm{mean}}$ was reduced but remained above the normal range even after deconvolution, thus intensity scaling and model inaccuracies are not sufficient to explain the poor agreement between the measured and predicted spectra. To further investigate the reasons behind the poor prediction accuracy of the remaining six outliers, we included contributions from the AA side chains, by calculating the CD spectra using four mixed basis sets (DS-dTSC3, DSSP-1SC3, HBSS-3SC1, and DS5-4SC1) Side-chain corrections eliminated two more proteins – Jacalin (SP175/41) shown in Fig S3D and Carbonic anhydrase (SP175/14) – from the list of outliers, reducing $RMSD_j^{\mathrm{mean}}$ of the predicted spectra by ~1.0 kMRE in both cases.

Closer inspection of the reference structures also revealed some common features that allowed us to speculate on possible reasons behind their poor obtained *RMSD* values. Four out of six outlier structures include Zn^{2+} or Fe^{2+} ions coordinated to histidine, glutamate, and aspartate side chains. These coordination centers likely have their own contribution to the CD spectrum, which is not accounted for in our predictions, and increases $RMSD_j^{\mathrm{mean}}$ for these proteins.

Additionally, five out of six outlier proteins proteins – except for hemerythrin (TS8/1) – have an unusually high fraction of turn structures, which is represented in a very coarse-grained way in our smaller optimized basis sets. Indeed, when the spectra were deconvolved using the DS5-4SC1 basis set which has three basis spectra dedicated to these structures $RMSD_j$ for four of the six – except for hemerythrin and insulin (SP175/40) – proteins were in the normal range.

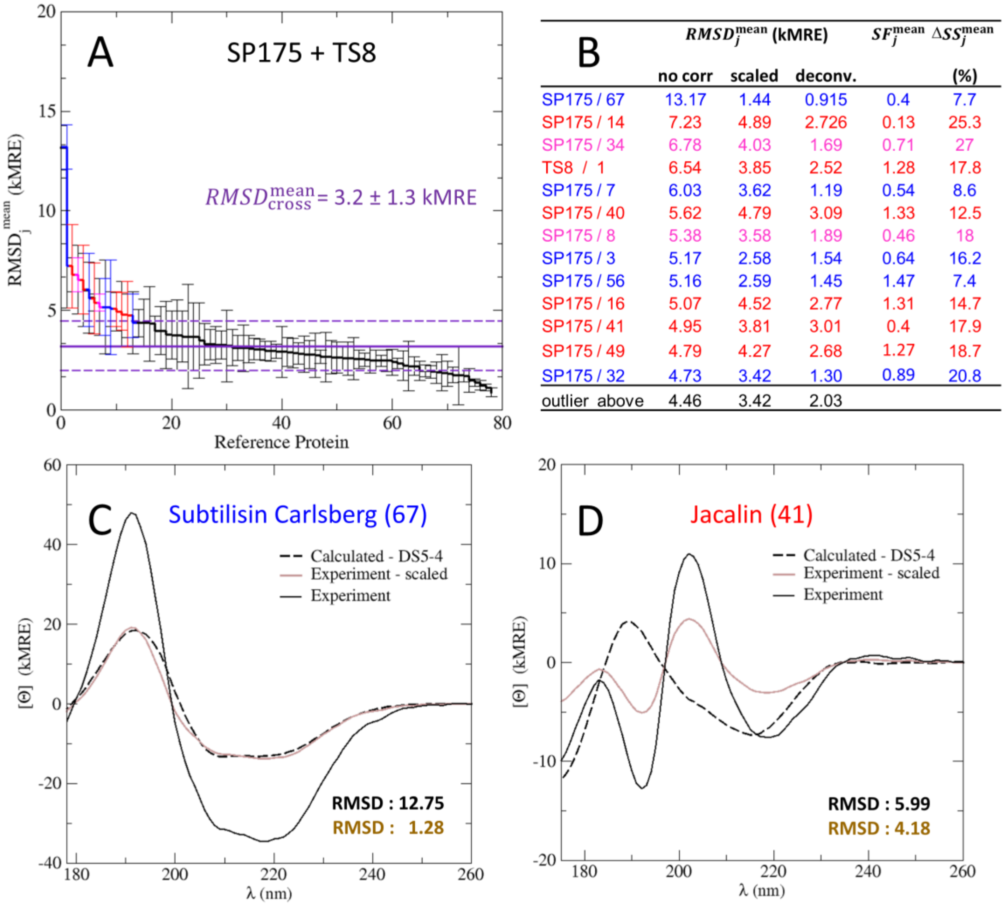

B	$RMSD_j^{\mathrm{mean}}$ (kMRE)			SF_j^{mean}	$\Delta SS_j^{\mathrm{mean}}$
	no corr	scaled	deconv.		(%)
SP175 / 67	13.17	1.44	0.915	0.4	7.7
SP175 / 14	7.23	4.89	2.726	0.13	25.3
SP175 / 34	6.78	4.03	1.69	0.71	27
TS8 / 1	6.54	3.85	2.52	1.28	17.8
SP175 / 7	6.03	3.62	1.19	0.54	8.6
SP175 / 40	5.62	4.79	3.09	1.33	12.5
SP175 / 8	5.38	3.58	1.89	0.46	18
SP175 / 3	5.17	2.58	1.54	0.64	16.2
SP175 / 56	5.16	2.59	1.45	1.47	7.4
SP175 / 16	5.07	4.52	2.77	1.31	14.7
SP175 / 41	4.95	3.81	3.01	0.4	17.9
SP175 / 49	4.79	4.27	2.68	1.27	18.7
SP175 / 32	4.73	3.42	1.30	0.89	20.8
outlier above	4.46	3.42	2.03		

Figure S3: Outliers of the SP175 and TS8 reference data sets. A) Reference proteins sorted by the mean deviation ($RMSD_j^{\mathrm{mean}}$) between their measured reference CD spectrum and spectra calculated from their reference structure. Proteins were selected as outliers if their $RMSD_j^{\mathrm{mean}}$ are by more than one standard deviation (dashed purple lines) larger than the mean prediction accuracy ($RMSD_{\mathrm{cross}}^{\mathrm{mean}}$, purple solid line) of the TS8 set. To determine the problem with the outliers their measured spectrum was scaled to match the predicted spectra, then deconvolved to find the SS composition that fits the spectrum best. B) List of the mean $RMSD$ values for the thirteen outliers in the two data sets, including their set and ID number, $RMSD_j^{\mathrm{mean}}$ before

corrections (no corr), after scaling (scaled), and subsequent deconvolution (deconv), along with the used scaling factor (SF_j^{mean}), and the calculated SS error of the structural model ($\Delta SS_j^{\mathrm{mean}}$). Outlier proteins in the figure are colored blue if their large *RMSD* is mostly due to incorrect intensity scaling, magenta if it is due to scaling combined with model inaccuracies, and red otherwise. C) Example protein 1: significant *RMSD* improvement by scaling the experimental CD spectrum and D) Example protein 2: where scaling could not improve the *RMSD* significantly. For panels C and D the experimental CD spectrum is shown as a solid black line, the rescaled experimental spectrum is shown as a solid brown line, and the spectrum calculated by the SESCA basis set DS5-4 is shown as a black dashed line. The name and ID number of the protein is shown on the top of the panel, while the *RMSD*s for the predicted spectra in kMRE units are shown on the bottom in black and brown respectively.

S10 Amino acid side-chain contributions in the far UV range

We derived the average contribution of side-chain groups to the CD signal of proteins as described in Section S3 from a new mixed reference set (MP79), which included 59 globular proteins of the SP175 reference set and a set of 20 tri-peptides designated as GXG20 set (where ‘X’ stands for one of the twenty natural AAs). As shown in Fig. S4A, the CD spectra of the GXG20 peptide set differ substantially from one another, despite the fact that the peptides were too short to form the hydrogen bonds required for stable α-helices and β-sheets, and therefore mostly adopted a random coil structure. We therefore assumed that the spectra of these peptides are largely defined by their single side-chain group. The GXG20 spectra already indicate that aromatic side groups – and particularly phenyl-alanine and tyrosine – have strong positive contributions to the CD spectra, which differs from the signals of other side chains. The CD spectrum of the GAG peptide, on the other hand, shows the largest negative peak at ~195 nm, similar to CD signal that is associated with a random coil protein, whereas the CD signal of the GGG peptide – in the absence of a chirality center – is very weak.

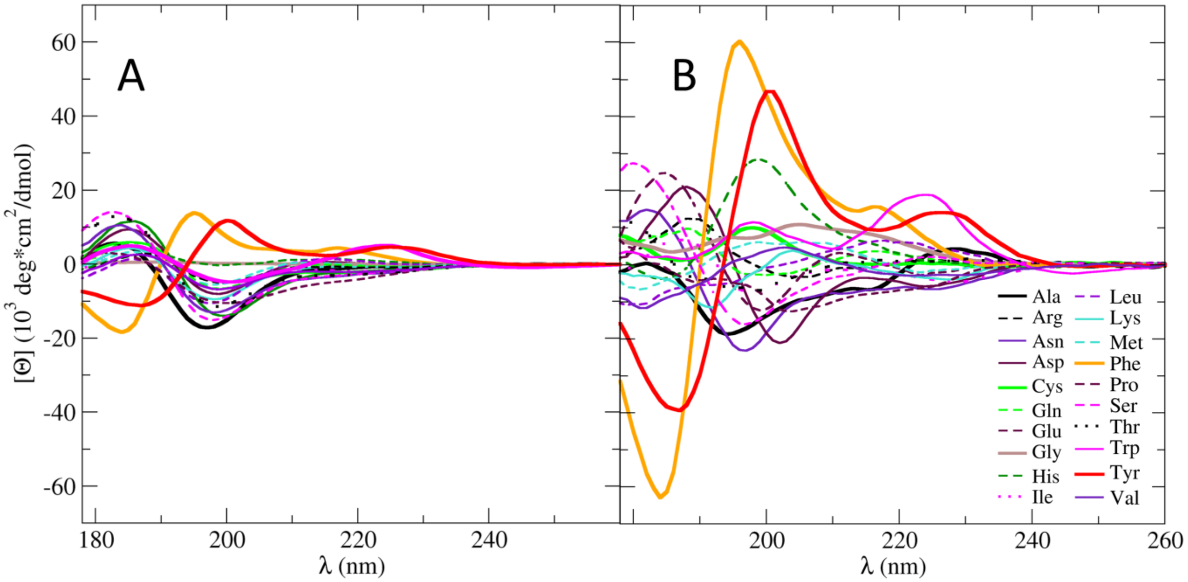

Figure S4: Circular dichroism contribution of AA side chains. A) Experimentally measured CD spectra measured at neutral p*H* for the 20 Ac-GXG-NH_2 peptides (GXG20). B) Calculated side-chain contributions for each AA side chain, derived from the SS composition and CD spectra of 59 globular proteins and the GXG20 peptides. The (CD/basis) spectra are color coded according to the AA side-chain groups they represent.

The pure basis spectra we derived from MP79 reference set (Fig S4B) are significantly larger than the CD spectra of the independent AAs (due to the normalization for the number of residues), and confirm the large contributions of the phenyl-alanine and tyrosine side chains. In addition, the basis spectra show moderate contributions from the AA side groups of asparagine, aspartate, glutamate, histidine, serine, and tryptophan, while the side chains of other AAs such as valine, isoleucine, and threonine had weaker CD signals.

We note that the GXG20 CD spectra differed considerably from the spectra of isolated amino acids measured by Nisihno *et al* [6]. at neutral, acidic and basic *pH*. In Fig. S32 we compare the two sets of CD spectra at neutral *pH* (7.0), where – despite the differences – the strongest signals were observed for phenyl-alanine, tyrosine, tryptophan. We also note that no reducing agent was added to GCG peptide during its CD measurements, and cysteine oxidation states (particularly cysteines forming disulfide bonds) were not considered separately.

S11 Analysis of the PCA basis sets

We determined the best achievable accuracy for a given number of basis spectra from basis sets that were constructed from the eigenvectors of a PCA of the SP175 reference CD spectra as described in Section S5. The first ten obtained PCA basis spectra are illustrated in Fig. S5A. In line with previous results [7–9], the first two PCA basis spectra are similar to the CD spectrum of purely α-helical and β-sheet proteins, and represent already about 94% of the variance within the spectra of the reference data set. As the sorted eigenvalues (Fig. S5B) suggest, only a few basis spectra should be required to achieve good to very high accuracy. Indeed, almost 99% of the variance of the SP175 CD spectra are represented by only the first five basis spectra, and the first ten basis spectra essentially describe the full data set. This expectation is confirmed in Fig. S5C, showing the reconstruction of the α-amylase precursor spectrum (SP175/3) using one to ten PCA basis spectra. For this spectrum already the first three basis spectra allow a good reconstruction with an average *RMSD* of 2.105 kMRE units (10^3 deg*cm^2/dmol), and using more than six or seven basis spectra essentially recovers the reference spectrum. For comparison, the average spectrum is shown in brown, corresponding to using no basis spectra at all, and serving as a lower limit of how well the spectra can be 'predicted' without any information. The table in Fig. S5D quantifies the changes in fitting accuracy for three sample spectra, taken from representative proteins of the three main structure classes (α-helical, β-sheet, and mixed α/β) and also provides the average *RMSD* for all 71 spectrum reconstructions (*RMSD*_ref).

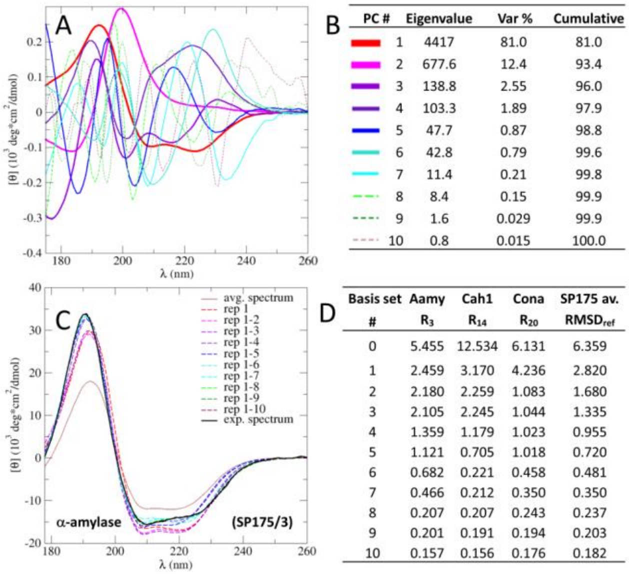

	PC #	Eigenvalue	Var %	Cumulative
▬	1	4417	81.0	81.0
▬	2	677.6	12.4	93.4
▬	3	138.8	2.55	96.0
▬	4	103.3	1.89	97.9
▬	5	47.7	0.87	98.8
▬	6	42.8	0.79	99.6
▬	7	11.4	0.21	99.8
- - -	8	8.4	0.15	99.9
- - -	9	1.6	0.029	99.9
- - -	10	0.8	0.015	100.0

Basis set	Aamy	Cah1	Cona	SP175 av.
#	R_3	R_{14}	R_{20}	$RMSD_{ref}$
0	5.455	12.534	6.131	6.359
1	2.459	3.170	4.236	2.820
2	2.180	2.259	1.083	1.680
3	2.105	2.245	1.044	1.335
4	1.359	1.179	1.023	0.955
5	1.121	0.705	1.018	0.720
6	0.682	0.221	0.458	0.481
7	0.466	0.212	0.350	0.350
8	0.207	0.207	0.243	0.237
9	0.201	0.191	0.194	0.203
10	0.157	0.156	0.176	0.182

Figure S5: Principal component analysis of the SP175 protein CD spectra. A) graphical representation of the first 10 principal component vectors sorted by their contribution to the spectral variance. B) Eigenvalue, contribution to variance, and cumulative contribution to the spectral variance for the same PC vectors. C) Reconstruction of the CD spectrum of α-amylase (Aamy) by its projection on the first 0-10 PC vectors. The original spectrum is shown in black, the average spectrum of SP 175 data set is shown in brown. The reconstructed spectra are shown as colored dashed lines. D) *RMSD* between the reconstruction of three selected proteins – α-amylase, carbonic anhydrase I (Cah1), and Concanavalin A (Cona) – and their original CD spectrum as function of PC vectors used. The column SP175 av. shows average *RMSD* for all 71 proteins in the data set.

To determine how much the SS elements and side chains contribute to the variance of CD spectra in the SP175 reference set, we also analyzed the correlations between the principal components describing the shape of the CD spectra (see Section S5) and the occurrence of AAs and SS elements in the reference proteins. To this aim, we calculated the Pearson correlation coefficients between the projections of the first ten PC vectors, the AA composition of the proteins, as well as the SS compositions determined by the BeStSel, DISICL, DSSP and HBSS algorithms.

Table S11 shows those structural properties which correlate most strongly with the principal components (PCs) of the CD spectra. As can be seen, the first three principal components involve mainly SS elements: PC 1 – which accounts for over 80% of the spectral variance of the reference set – was very strongly correlated ($R_{pearson}$ ~0.9) to the presence of α-helices in the protein structure, whilst PC 2 and 3 are moderately correlated to β-strand and turn structures. However, PCs 4, 6, 9, and 10 correlate more strongly with the presence of AAs than SS elements. Since these principal components describe ~3% of the spectral variance, one would expect a somewhat smaller but still notable contribution from side-chain groups. In addition, the most commonly considered correction to CD spectra are associated with the aromatic side chains of tryptophan, phenyl-alanine, and tyrosine because these AAs have the strongest CD signals in isolation. Our analysis also suggests that AA side chains with weaker CD activity, particularly arginine, histidine, cysteine and serine, may also contribute significantly to the CD spectra.

S12 Model validation for the P53/CBP complex

The quality of the structure models was determined through cross-validation by predicting the NMR chemical shifts from both structural models (NMR and MD) and then comparing the results to the experimental chemical shifts from the original NMR measurements (obtained from biological magnetic resonance databank, entry no. 17073). We computed the backbone chemical shifts (including those for the N, C_{α}, C_{β}, C, H_{N}, and H_{α} atoms) using the chemical shift predictor Sparta+ [10]. Figure S6A shows the comparison between the experimental and calculated C_{α} secondary chemical shifts. Secondary chemical shift values are corrected for the average random coil chemical shift of the AA, and therefore indicative of the local protein (secondary) structure. A sequence of large positive secondary C_{α} shifts indicates a high propensity for α-helix in that region, whilst a sequence of large negative values shows a preference towards β-strands or extended structures. The overall agreement between the measured and predicted chemical shifts was quantified the through average *RMSD* of their secondary chemical shift profiles.

The comparison in Fig. S6A also revealed that the *RMSD* of the MD ensemble C_{α} chemical shifts (1.06 ppm) was lower than that of the NMR bundle (1.39 ppm). The same trends were observed for the average *RMSD* of all backbone chemical shifts as well. The C_{α} chemical shifts also indicate that our models agree well with the experimental chemical shifts on the position of the helical regions, but overestimate the helix propensities, especially for the C-terminal helix of CBP-NCBD, and the helical regions in P53-AD2. These regions are also the ones where the average SS composition is considerably less helical in the MD ensemble than in the NMR bundle. Additionally, the residues of the short β-sheets observed only in the MD model possess some of the largest negative C_{α} secondary chemical shifts of the experimental profile, suggesting that presence of these β-sheets also contribute to the lower average *RMSD* of the MD model.

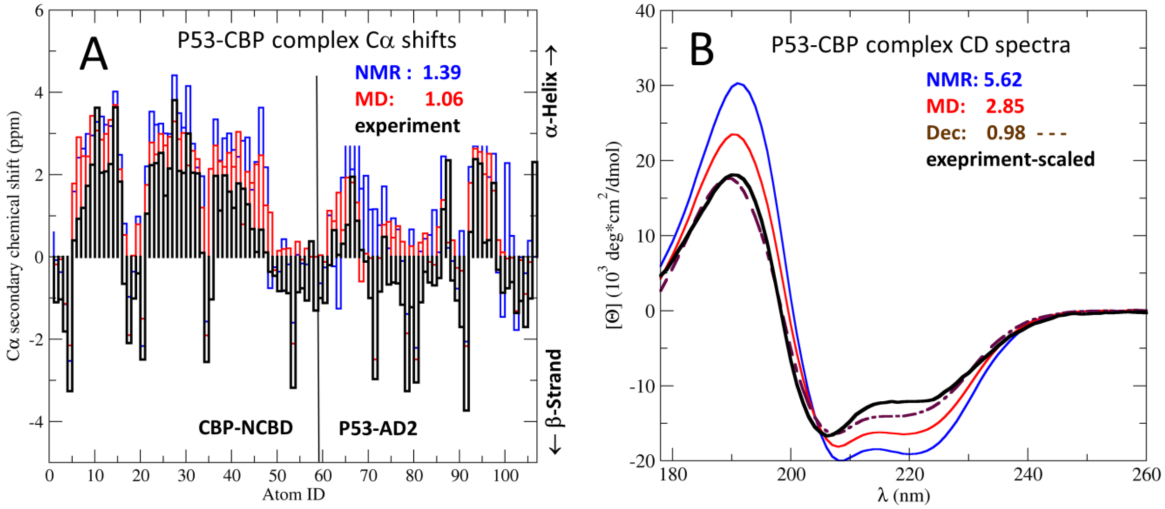

Figure S6: Model validation by comparison to experimental observables. The measured observables (experiment) were compared to the same observables calculated from two structural models (NMR and MD). Panels of the figure show the comparison of A) the Cα secondary chemical shifts and B) the CD spectra, respectively. The measured observables are shown as black solid lines, calculated observables are shown in different colors according to the underlying model. The dashed spectrum in B) shows the prediction from the ideal SS composition determined by spectrum deconvolution (Dec). The average *RMSD* from the experimental observable (in ppm and mean residue ellipticity units, respectively) for each model is shown in the corresponding color. The CD spectra in B) were calculated using the DS-dTSC3 basis set, and include side-chain corrections.

We also analyzed the differences in the SS composition of the two models. A summary over SS composition of each structural model is shown below their cartoon representation in Fig. 8A. As the figure shows, about 47% of the residues in the NMR are in an α-helical conformation. Although no β-sheets appeared in this model, a low percentage AAs adopted a local conformation typical for an extended β-strand at the termini of the two protein domains.

The P53/CBP complex was very dynamic during the MD simulations. The two domains remained strongly bound during the simulation, but the conformational fluctuations resulted in a 38% average α-helix content. In addition, while the total β-strand content decreased slightly in the MD model compared to the NMR bundle, 2.8% of the residues in the MD model was in a regular β-strand conformation, and established the hydrogen bonds to form two short β-sheets which appeared with ~15% probability in the ensemble. These short β sheets connected the N-terminus of CBP-NCBD with residues 25-27 of P53-AD2, and the two termini P53-AD2. Predicting CD spectra from these SS compositions (Fig. S6B) suggested similar trends observed for the C_α secondary chemical shifts, whereas deconvolution of the measured CD spectrum indicated an ideal SS composition that is 8-10% less helical than that of the MD model.

Additional Supplementary Tables:

Table S1: The SP175 dataset. Identification number (ID), abbreviation (short code), protein databank (pdb) code, protein circular dichroism databank (pcddb) code, and name for each of the proteins in the dataset is provided, as well as number residues (size) and resolution (resol.) of the model structure. For further details see ref. [11]. Entries marked by plus signs in the ID sections (and highlighted in red) were part of the SP175 dataset, but not part of the TR64 dataset, whilst entries marked by stars (and highlighted in blue) were part SP175 but not part of the GP59 dataset

ID number	short code abbrev.	structure pdb code	CD spectrum pcddb code	Protein Name	Size (res)	resol. (A)
1	Aldo	1ado	CD0000001	Aldolase	1452	1.90
2	alkp	1ed9	CD0000002	Alkalnie phosphatase	898	1.75
3*	aamy	1vjs	CD0000003	Alpha amylase prec	469	1.70
4	abun	1hc9	CD0000004	Alpha-bungarotoxin	173	1.80
5	actp	5cha	CD0000005	Alpha Chymotrypsin	474	1.67
6	actn	2cga	CD0000006	Alpha chymotrypsinogen	490	1.80
7*	ptib	5pti	CD0000007	Pancreatic trypsin inhibitor (bov.)	58	1.00
8*	avdn	1rav	CD0000008	Avidin (recombinant)	248	2.20
9	bamy	1fa2	CD0000009	Beta amylase (sweet potato)	498	2.30
10	bglc	1bgl	CD0000010	Beta galactosidase	8168	2.50
11	blac	1b8e	CD0000011	Beta lactoglobulin (bovine)	152	1.95
12	cphy	1ha7	CD0000012	C-phycocyanin	3996	2.20
13	calm	1lin	CD0000013	Calmodulin	146	2.00
14*	cah1	1hcb	CD0000014	Carbonic anhydrase I	258	1.60
15	cah2	1v9e	CD0000015	Carbonic anhydrase II (bovine)	518	1.95
16*	carp	5cpa	CD0000016	Carboxypeptidase	307	1.54
17	ecat	1dgf	CD0000017	Erythrocyte catalase (human)	1998	1.50
18	cerp	1kcw	CD0000018	Ceruloplasmin (human)	1017	3.00
19	cits	2cts	CD0000019	Citrate synthase	437	2.00
20+	cona	1nls	CD0000020	Concanavalin A	237	0.94
21+	cytc	1hrc	CD0000021	Cytochrome C (horrse heart)	104	1.90
22	bbcr	2bb2	CD0000022	Beta b2 crystallin (bovine)	176	2.10
23	gbcr	4gcr	CD0000023	Gamma b crystallin (bovine)	174	1.47
24	gdcr	1elp	CD0000024	Gamma d crystalline	346	1.95
25	gecr	1m8u	CD0000025	Gamma e crystallin (bovine)	173	1.65
26	gscr	1ha4	CD0000026	Gamma S crystallin C-term (human)	174	2.40
27	gdc2	1hk0	CD0000027	Gamma d crystallin (human)	173	1.25
28	dqd1	1qfe	CD0000028	Dehydroquinate dehydratase I (S. Thypi)	504	2.10
29	dqd2	2dhq	CD0000029	Dehydroquinate dehydratase I (M. Tuber)	136	2.00
30	dna1	3dni	CD0000030	Dnase I	258	2.00
31	pela	3est	CD0000031	Pancreatic elastase	229	1.65
32*	fesf	2fdn	CD0000032	2[4Fe-4S] ferredoxin	55	0.94
33	glco	1cf3	CD0000033	Glucose oxidase	581	1.90
34*	gldh	3mw9	CD0000034	Glutamate dehydrogenase (bovine)	3009	2.40

Table S1: The SP175 dataset (cont.)

ID	short code	structure	CD spectrum	Protein	Size	resol.
number	abbrev.	pdb code	pcddb code	Name	(res)	(A)
35	glps	1gpb	CD0000035	Glycogen phosphorylase	823	1.90
36	hadh	1bn6	CD0000036	Haloalkaene dehalogenase	291	1.50
37+	hglb	1hda	CD0000037	Hemoglobin (human)	572	2.20
38	hsa1	1n5u	CD0000038	Serum Albumin (human)	583	1.90
39	igg2	1igt	CD0000039	Immunglobulin G2a (mouse)	1300	2.80
40*	hins	1trz	CD0000040	Insulin A&C (human)	102	1.60
41*	jaca	1ku8	CD0000041	Jacalin	596	1.75
42	lacf	1blf	CD0000042	Lactoferrin (bovine)	685	2.80
43	lect	1les	CD0000043	Lectin (lentil)	458	1.90
44	lept	1ax8	CD0000044	Leptin E100 (human)	130	2.40
45+	lysm	193l	CD0000045	Lysozime (hen, egg-white)	129	1.33
46	moll	1mol	CD0000046	Mollein	188	1.70
47	mmyo	1ymb	CD0000047	Metmyoglobin	153	1.90
48+	Mglb	1a6m	CD0000048	Myoglobin (oxy)	151	1.00
49*	Nmra	1k6j	CD0000049	Nmra trans. Regulator	634	1.80
50	Oalb	1ova	CD0000050	Ovalbumin	1446	1.95
51	Otrn	1dot	CD0000051	Ovotransferrin (duck)	686	2.35
52+	Papn	1ppn	CD0000052	Papain (papaya)	212	1.60
53	lec2	1ofs	CD0000053	Lectin (pea)	460	1.80
54	Plyc	1air	CD0000054	Pectate lyase C	352	2.20
55	Peps	2psg	CD0000055	Pepsinogen	326	1.80
56*	pox1	7atj	CD0000056	Peroxydase C1A (horse-raddish)	305	1.47
57	Pgmu	3pmg	CD0000057	Phosphoglucomuatse (rabbit)	1120	2.40
58	Pgkn	3pgk	CD0000058	Phosphoglycerate kinase	415	2.50
59	pla2	1une	CD0000059	Phospholipase A2 (bovine)	123	1.50
60	Pemt	1hnn	CD0000060	Phenylethanolamine N-methyltransferase	528	2.40
61	Pkin	1a49	CD0000061	Pyruvate kinase	4152	2.10
62	Rhod	1rhs	CD0000062	rhodanase (sulphur-subst, bovine)	292	1.36
63+	Rnas	3rn3	CD0000063	Ribonuclase A (bovine)	124	1.45
64	Rubr	1r0i	CD0000064	Rubredoxin (Cadmium subs)	53	1.50
65	tpi2	1ba7	CD0000065	Trypsin inhibitor (soy bean)	334	2.50
66	Stvn	1stp	CD0000066	Streptavidin	121	2.60
67*	subc	1scd	CD0000067	Subtilisin Carlsberg (crosslinked)	247	2.30
68	cttp	1cgj	CD0000068	Chmyotrypsinogen A + Trypsin inhibitor	301	2.30
69	thau	1thw	CD0000069	Thaumatin	207	1.75
70	tpis	7tim	CD0000070	Triosephosphate isomerase	494	1.90
71	ubqn	1ubi	CD0000071	ubiquitin (human)	76	1.80

Table S2: The TS8 globular protein cross -validation protein set Identification number (ID), abbreviation (short code), RSCB protein databank (pdb) code, circular dichroism filename, and name for each of the proteins in the dataset is provided, as well as number residues (size) and resolution (resol.) of the model structure. The CD spectra of this dataset were extracted from the globular protein training set provided with the CCA deconvolution program of Hollósi et al. See ref.[2] for further details.

ID	short code	structure	CD spectrum	Protein	Size (res)	resol.
number	abbreviation	pdb code	short code	Name	(res)	(A)
1	Hmrt	4xpx	CD_HMRT.dat	Hemerythrin	130	1.03
2	Azu	5azu	CD_AZU.dat	Azurin	512	1.90
3	Pral	2pab	CD_PRAL.dat	Prealbumin	228	1.80
4	Ldh	6ldh	CD_LDH.dat	Lactate dehydrogenase	329	2.00
5	Thml	8tln	CD_THML.dat	Thermolysin	318	1.60
6	Gpd	3gpd	CD_GPP.dat	Phosphate dehydrogenase	668	3.5
7	Subn	1sbt	CD_SUBN.dat	Subtilisin novo	275	2.50
8	Tnf	2tnf	CD_TNF.dat	Tumor necrosis factor alpha	444	1.40

Table S3: The EV9 evaluation protein dataset. Identification number (ID), abbreviation (short code), RSCB protein databank (pdb) code, circular dichroism filename, and name for each of the proteins in the dataset is provided, as well as number residues (size) and resolution (resol.) of the model structure. The CD spectra of this dataset were extracted from the globular protein training set provided with the CCA deconvolution program of Hollósi et al. See ref. [2] for further details.

ID	short code	structure	CD spectrum	Protein	Size (res)	resol.
number	abbreviation	pdb code	short code	name	(res)	(A)
1	mglb	1vxf	CD_MGLB.out	Myoglobin	153	1.70
2	hglb	2mhb	CD_HGLB.out	Hemoglobin	287	2.00
3	cytc	5cyt	CD_CYTC.out	Cytochrome C	103	1.50
4	lysm	4lzt	CD_LYSM.out	Lysozyme	129	0.95
5	papn	9pap	CD_PAPN.out	Papain	211	1.65
6	rnas	1rbx	CD_RNAS.out	Ribonuclease A	124	1.69
7	bnjn	1rei	CD_BNJN.out	Benes-Jones peptide	214	2.00
8	cona	1nls	CD_CONA.out	Concanvallin A	237	0.94
9	suds	1sxn	CD_SUDS.out	Superoxide dismutase	302	1.90

Table S4: Secondary structure elements recognized by the structure classification algorithm DSSP (see ref [12]). DSSP recognizes SS elements based on backbone hydrogen bond patterns. Note that the 4-Helix class represents the regular α-helix, while 3-Helix and 5-Helix is associated with the distorted 3_{10}- and π-helices, respectively.

DSSP secondary structure classes		
Struct. Element	**K**	**Abbr.**
4-Helix	1	4H
Beta-Strand	2	BS
3-Helix	3	3H
5-Helix	4	5H
Beta-Bridge	5	BB
Bend	6	BE
Turn	7	TU
Unclassified	8	UC

Table S5: Secondary structure elements recognized by the structure classification algorithm DISICL (see ref [13]). DISICL recognizes SS elements based on backbone dihedral angles in short segments of the protein, to provide a better resolution on loop- and turn structures.

Detailed DISICL classes			**Simplified DISICL classes**		
Struct. Element	**K**	**Abbr.**	**Struct. Element**	**abbr.**	**i**
α-Helix	1	ALH	Helical	HEL	1
π-Helix	2	PIH	Helical	HEL	1
Helix-Cap	3	HC	Helical	HEL	1
extended β-Strand	4	EBS	β-Strand	BS	2
normal β-Strand	5	NBS	β-Strand	BS	2
β-Cap	6	BC	β-Strand	BS	2
Turn type 2	7	TII	β-Turn	BT	3
Turn type 8	8	TVIII	β-Turn	BT	3
Turn type 1	9	TI	3-Helical Turn	3HT	4
3_{10} Helix	10	3H	3-Helical Turn	3HT	4
Turn-Cap	11	TC	3-Helical Turn	3HT	4
Poly-proline Helical	12	PP	Irregular b	IRB	5
Bulge	13	Bu	Irregular b	IRB	5
Left-handed Helix	14	LHH	Left-Handed Turns	LHT	6
Left-handed Turn II	15	LTII	Left-Handed Turns	LHT	6
Haripin 2:2	16	HP	Other Tight Turns	OTT	7
γ-Turn	17	GXT	Other Tight Turns	OTT	7
Schellmann-Turn	18	SCH	Other Tight Turns	OTT	7
Unclassified	19	UC	Unclassified	UC	8

Table S6: Secondary structure elements recognized by the structure classification algorithm HbSS. This algorithm recognizes SS elements based on backbone hydrogen bond patterns, similarly to DSSP. In addition, it can identify parallel and anti-parallel β-strands (see Fig. S2), and further distinguish strand handedness (based on β-strand twist angles) to be more comparable to BeStSel algorithm (see ref [3]).

Extended HbSS classes			**HbSS secondary structure classes**		
Struct. Element	**K**	**Abbr.**	**Struct. Element**	**K**	**Abbr.**
α-Helix	1	4H	α-Helix	1	4H
3/10Helix	2	3H	3/10Helix	2	3H
π-Helix	3	5H	π-Helix	3	5H
Left-twist. parallel β	4	LHP	Parallel β-strand	4	BSP
Non-twist. parallel β	5	NBP	Parallel β-strand	4	BSP
Right-twist. parallel β	6	RHP	Parallel β-strand	4	BSP
Left-twist. anti-par. β	7	LHA	Anti-par. β-strand	5	BSA
Non-twist. anti-par. β	8	NBA	Anti-par. β-strand	5	BSA
Right-twist. anti-par. β	9	RHA	Anti-par. β-strand	5	BSA
H-bonded Turn	10	TU	H-bonded Turn	6	TU
Unclassified	11	UNC	Unclassified	7	UNC

Table S7: Secondary structure elements recognized by the CD deconvolution algorithm BeStSel (see ref [3]). This deconvolution basis set was derived from the SP175 set, to provide a better resolution on β-strand SS elements. Note that the 'Irregular Helix' class is associated with the distorted ends of a regular α-helix, and the classical 3_{10}-helix was assigned to the 'Other' class

BeStSel deconvolution basis spectra		
Struct. Element	**k**	**Abbr.**
α-Helix	1	Helix1
Irregular Helix	2	Helix2
Left-twist anti-par. β	3	LHA
Relaxed anti-par. β	4	NBA
Right-twist anti-par. β	5	RHA
Parallel β-strand	6	NBP
Turns	7	Turn
Other	8	Other

Table S8: Calculated accuracy of top-ranking optimized basis sets based on protein SS composition. The table shows the name of the basis set, the number of basis spectra (size), the average root mean square deviation (*RMSD*) between the experimental and calculated CD spectra for four protein reference sets (SP175, TR64, EV9, TS8). Basis sets in the table were derived using SP175 set and cross-validated on the TS8 set. The type section describes the underlying SS classification protocol used to derive the basis set (DS_sim, DS_det, Dssp, HBSS, or HBSS_ext, see Section 3.4 for details).

Basis spectrum set			***RMSD*$_{set}$ (kMRE)**			
Name	**Type**	**size**	**SP175**	**TR64**	**EV9**	**TS8**
DS3-1	DS_sim	5	3.804	3.93	2.998	3.396
DS3-3	DS_sim	4	3.823	3.921	3.262	3.455
DS5-4	DS_det	6	3.657	3.764	2.582	3.475
DS6-1	DS_det	6	3.441	3.525	3.402	3.422
DS-dT*	DS_det	3	3.899	4.007	3.131	3.146
DSSP-1*	Dssp	4	3.985	4.104	3.175	2.992
DSSP-T	Dssp	3	4.024	4.138	3.274	3.008
HBSS-2	HBSS_ext	6	3.924	3.979	3.603	3.66
HBSS-3*	HBSS_ext	5	3.982	4.028	3.75	3.295
HBSS-4	HBSS	4	4.104	4.206	3.421	3.622
DS_simF	DS_sim[I]	8	3.655	3.777	3.19	3.487
DS_detF	DS_det[I]	19	2.922	2.959	3.896	4.148
DSSP-F	Dssp[I]	8	3.75	3.806	3.4	3.038
HBSS-E	HBSS_ext[I]	11	3.919	3.971	3.591	3.64
HBSS-F	HBSS[I]	7	3.568	3.648	3.221	4.272
Sreer-1	DS_det[D]	6	7.614	7.573	6.916	5.154
Perczel-1	DS_det[D]	5	4.717	4.88	3.562	4.416
Perczel-2	Dssp[D]	5	4.819	4.947	3.69	3.405

*: most predictive basis set found for a given classification algorithm.

[D]: basis spectra were determined by deconvolution methods previously, and not computed in this study.

[I]: non-optimized initial basis sets.

Table S9: Calculated accuracy for other CD spectrum prediction methods, and mixed basis sets. The table shows the name of the basis set or method, the number of number of backbone and side-chain basis spectra (size), the average root mean square deviation (*RMSD*) between the experimental and calculated CD spectra for four reference sets (MP79, GXG20, SP175, and TS8).). Basis sets in the table were derived using MP79 set and cross-validated on the TS8 set. The type section describes the underlying structure classification protocol for basis sets (DS_det, DSSP, or HbSS_ext) complemented by SC for side-chain corrections. For other methods: Best denotes a basis set is based on SS predicted from the CD spectra by the BeStSel algorithm, corresponds to the *RMSD* using perfect structural models. MatM stands for direct spectrum calculation with the matrix method, whereas SVM abbreviates an empirical spectrum calculation based on support vector machine techniques.

Basis spectrum set			***RMSD*$_{\text{set}}$ (kMRE)**			
Name	**Type**	**size**	**MP79**	**GXG20**	**SP175**	**TS8**
DichroCalc	MatM[C]	-----	-----	-----	6.692	5.568
PDB2CD	SVM[C,S]	-----	-----	-----	2.413	3.938
Bestsel_der	Best[S]	8+0	2.998	4.354	3.08	1.828
DS-dTSC3	DS_det+SC	3+4	3.048	2.402	3.925	2.951
DS5-4SC1	DS_det+SC	6+6	2.9	3.095	3.762	2.817
DS6-1SC1	DS_det+SC	6+6	2.804	2.876	3.575	2.907
DSSP-1SC3	DSSP+SC	4+6	3.247	3.39	4.052	2.849
DSSP-TSC1	DSSP+SC	3+6	3.33	3.495	4.128	2.901
HBSS-3SC1	HbSS_ext+SC	5+4	3.18	3.433	4.014	3.109
HBSS-3SCF	HbSS_ext+SC	5+20	2.837	3.376	3.969	3.263

[S]: method trained on the SP175 reference set.

[C]: competing method.

Table S10: The TS14 protein dataset. Identification number (ID), abbreviation (short code), RSCB protein databank (pdb) code, protein circular dichroism databank filename, and name for each of the proteins in the dataset is provided, as well as number residues (size) and resolution (resol.) of the model structure. The CD spectra of this dataset were used to repeat the cross-validation performed by Mavridis et al. See ref. [14] for further details.

ID	short code	structure	CD spectrum	Protein	Size	resol.
number	abbrev.	pdb code	short code	Name	(res)	(A)
1	a1at	1qlp	CD0003891000	Alpha-1-antitrypsin	394	2.0
2	atr3	1sr5	CD0003889000	Antithrombin-III	689	3.1
3	bcr2	1ytq	CD0003670000	Beta-crystallin B2	181	1.7
4	bcr3	1bd7	CD0003672000	Beta-crystallin B2	347	2.78
5	Bcr4	1oki	CD0003668000	Beta-crystallin B1	366	1.4
6	bcry	1a7h	CD0003669000	Gamma-crystallin S	172	2.56
7	bmgl	2yxf	CD0003894000	Beta-2-microglobulin	99	1.13
8	cxcn	2ccm	CD0004676000	Calexcitin	386	1.8
9	ectn	1ecz	CD0003896000	Ecotin	284	2.68
10	hutp	1q5u	CD0003897000	human dUTPase	390	2.0
11	ipdh	2y3z	CD0003898000	3-isopropylmalate dehydrogenase	351	1.8
12	magl	4acq	CD0003893000	Alpha-2-macroglobulin	5132	4.3
13	npta	2zxe	CD0001180000	Na/K transporting ATPase	1296	2.4
14	sctx	4kyp	CD0004244000	Beta-scorpion toxin	290	1.7

Table S11: Correlation analysis of the spectral components.

PC1	Corr.	Prop	Desc.	PC6	Corr.	Prop	Desc.
1	0.921	Hel1 (Best)	α-helix	1	0.201	SER (AA)	Amino A.
2	0.906	Hel1 (SEL)	α-helix	2	0.163	CYS (AA)	Amino A.
3	0.9	ALH (DISICL)	α-helix	3	0.138	RHA (HbSS)	Strand
4	0.898	Hel (DISICL)	α-helix	4	0.157	Hel2 (Best)	Helix
5	0.892	4H (DSSP)	α-helix	5	0.126	Hel1 (SEL)	α-helix
6	0.891	4H (HbSS)	α-helix	6	0.116	ALH (DISICL)	α-helix
PC2	**Corr.**	**Prop**	**Desc.**	**PC7**	**Corr.**	**Prop**	**Desc.**
1	0.532	EBS (DISICL)	β-strand	1	0.285	RHP (HbSS)	β-strand
2	0.513	Anti1 (Best)	β-strand	2	0.274	BSP (HbSS)	β-strand
3	0.444	NBA (HbSS)	β-strand	3	0.25	Para (Best)	β-strand
4	0.418	Anti2 (Best)	β-strand	4	0.23	Turn (Sel)	Turn
5	0.395	BS (HbSS)	β-strand	5	0.205	Bend (DSSP)	Turn
6	0.352	HIS (AA)	Amino A.	6	0.169	GXT (DISICL)	Turn
PC3	**Corr.**	**Prop**	**Desc.**	**PC8**	**Corr.**	**Prop**	**Desc.**
1	0.31	BS (HbSS)	β-strand	1	0.386	3H (DSSP)	Helix
2	0.299	SCH (DISICL)	Turn	2	0.344	3H (HbSS)	Helix
3	0.254	NBS (DISICL)	β-strand	3	0.3	5H (HbSS)	Helix
4	0.23	Bend (DSSP)	Turn	4	0.273	HC (DISICL)	Turn
5	0.216	NBA (HbSS)	β-strand	5	0.253	MET (AA)	Amino A.
6	0.205	THR (AA)	Amino A.	6	0.139	Other (Best)	Turn
PC4	**Corr.**	**Prop**	**Desc.**	**PC9**	**Corr.**	**Prop**	**Desc.**
1	0.471	ARG (AA)	Amino A.	1	0.223	ASP (AA)	Amino A.
2	0.397	LHH (DISICL)	Turn	2	0.202	3H(HbSS)	Helix.
3	0.306	Anti2 (Best)	β-strand	3	0.192	GLU (AA)	Amino A
4	0.293	NBA (HbSS)	β-strand	4	0.152	ILE (AA)	Amino A.
5	0.299	SCH (DISICL)	Turn	5	0.152	3H (DSSP)	Helix
6	0.272	LHT (DISICL)	Turn	6	0.126	PIH (DISICL)	Helix
PC5	**Corr.**	**Prop**	**Desc.**	**PC10**	**Corr.**	**Prop**	**Desc.**
1	0.394	3HT(DISICL)	Helix	1	0.214	PHE (AA)	Amino A.
2	0.376	3H (DISICL)	Helix	2	0.15	TRP (AA)	Amino A.
3	0.33	3H (DSSP)	Helix	3	0.14	SER (AA)	Amino A.
4	0.321	3H (HbSS)	Helix	4	0.133	RHA (HbSS)	β-strand
5	0.296	Cys (AA)	Amino A.	5	0.116	Bend (DSSP)	Turn
6	0.294	Hel2 (SEL)	Helix	6	0.102	LHT (DISICL)	Turn

The six best correlated structural properties are listed for each of the first ten principal components of the SP175 CD spectra. The table displays the abbreviated code of the structural property (Prop), the Pearson correlation score (Corr.) between the projections of the PC vector, and the coefficients of the structural property (the fraction of SS element or AA in a protein), as well as the type and a short description of the structural property. The type (in parenthesis) defines the source algorithm for SS elements (DSSP, HbSS, DISICL or BeStSel algorithms) and (AA) stands for amino acids. The short description shows if a SS element is either associated with α-helix, irregular helix (Helix), β-strand or turn structures.

Additional Supplementary Figures:

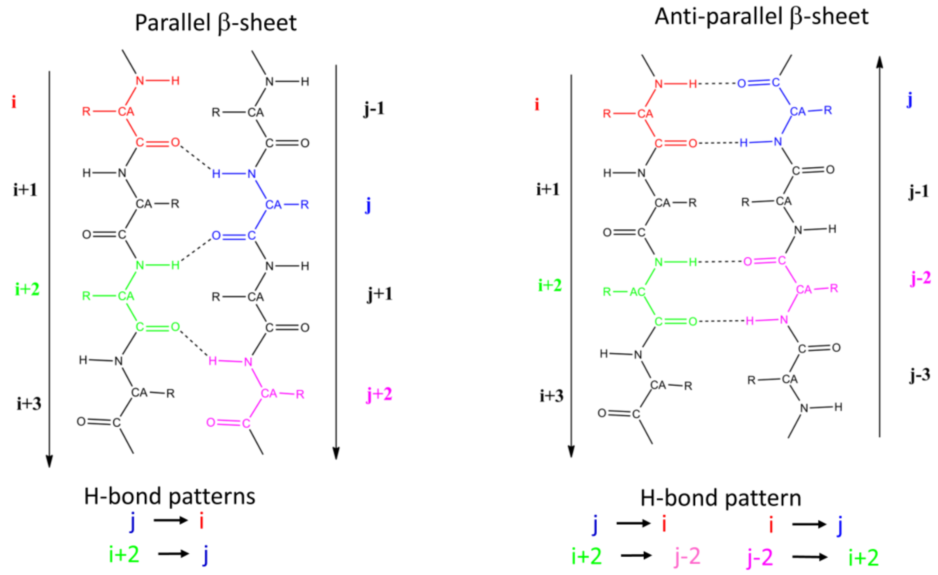

Figure S7: Definition of parallel and anti-parallel hydrogen bonding for the algorithm HbSS. The indicated AAs relative to the hydrogen bonded pair i and j are identified as a parallel or anti-parallel β-sheet, if hydrogen bonds indicated at the bottom are present. The arrows denote a hydrogen bond between N-H donor group on the left side and the C=O acceptor group on right side.

Map_DSSP-T	i	1	2	3
k	α_{ki}	Helix	Sheet	Coil
1	3H	1	0	0
2	4H	1	0	0
3	5H	1	0	0
4	BS	0	1	0
5	BB	0	0	1
6	TU	0	0	1
7	BE	0	0	1
8	UC	0	0	1

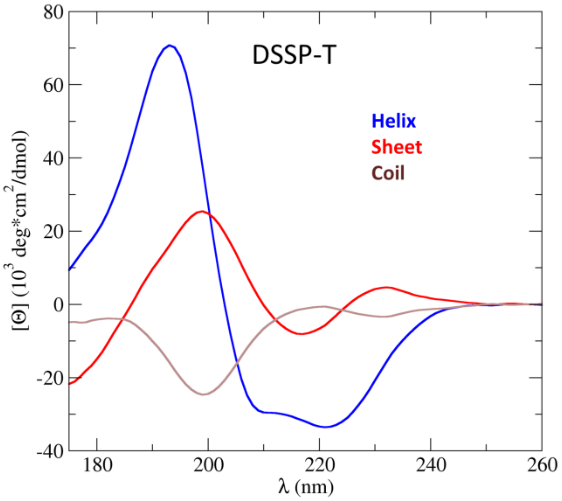

Figure S8: Assignment (left) and basis spectra (right) for the basis set DSSP-T. Secondary structure elements for the assignment are abbreviated according to Table S4.

Map_DSSP-1	i	1	2	3	4
k	α_{ki}	Helix	Beta	Bridge	Other
1	3H	1	0	0	0
2	4H	1	0	0	0
3	5H	0	1	0	0
4	BS	0	1	0	0
5	BB	0	0	1	0
6	TU	0	0	0	1
7	BE	0	0	0	1
8	UC	0	0	0	1

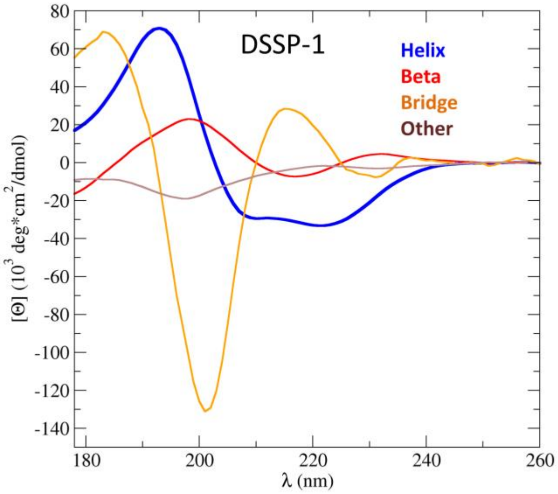

Figure S9: Assignment (left) and basis spectra (right) for the basis set DSSP-1. Secondary structure elements for the assignment are abbreviated according to Table S4.

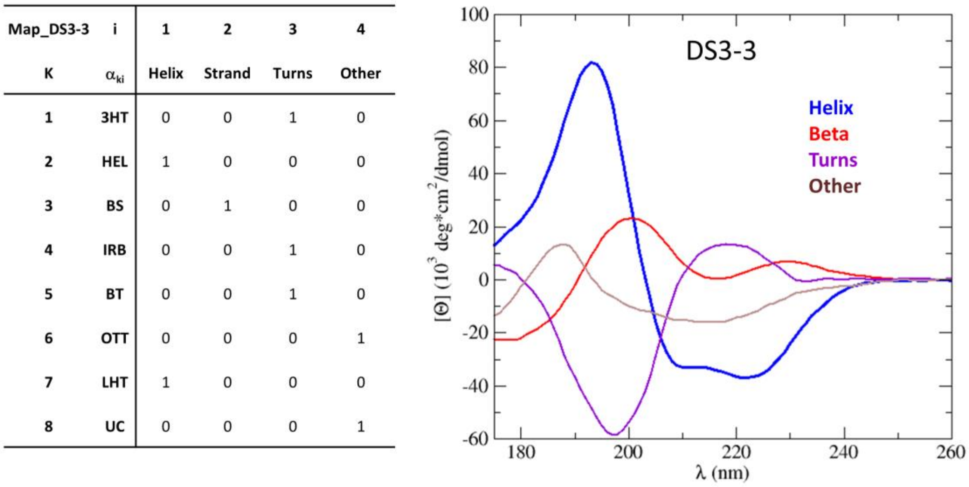

Map_DS3-3	i	1	2	3	4
K	α_{ki}	Helix	Strand	Turns	Other
1	3HT	0	0	1	0
2	HEL	1	0	0	0
3	BS	0	1	0	0
4	IRB	0	0	1	0
5	BT	0	0	1	0
6	OTT	0	0	0	1
7	LHT	1	0	0	0
8	UC	0	0	0	1

Figure S10: Assignment (left) and basis spectra (right) for the basis set DS3-3. Secondary structure elements for the assignment are abbreviated according to Table S5.

Map_DS-dT	i	1	2	3
k	α_{ki}	Helix	Beta	Coil
1	3H	1	0	0
2	ALH	1	0	0
3	PIH	1	0	0
4	EBS	0	1	0
5	NBS	0	1	0
6	PP	0	0	1
7	TI	0	0	1
8	TII	0	0	1
9	TVIII	0	0	1
10	GXT	0	0	1
11	SCH	0	0	1
12	HP	0	0	1
13	TC	0	0	1
14	HC	0	0	1
15	BC	1	0	1
16	BU	0	0	1
17	LTII	0	0	1
18	LHH	0	0	1
19	UC	0	0	1

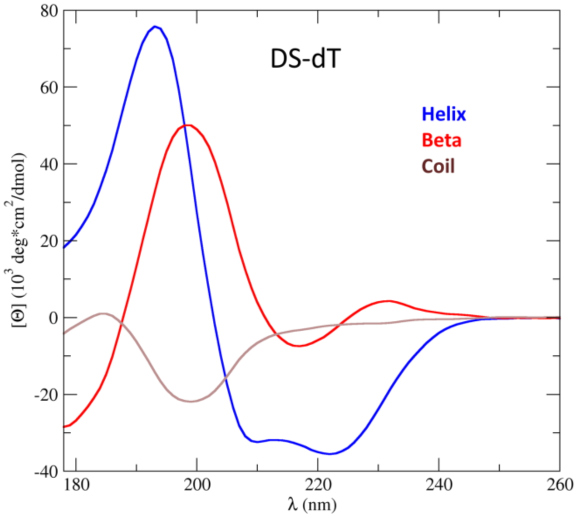

Figure S11: Assignment (left) and basis spectra (right) for the basis set DS-dT. Secondary structure elements for the assignment are abbreviated according to Table S5.

Map_DS5-4	i	1	2	3	4	5	6
k	α_{ki}	Helix-1	Beta-1	Helix-2	Turn-1	Turn-2	Other
1	3H	0	0	1	0	0	0
2	ALH	1	0	0	0	0	0
3	PIH	0	0	0	0	1	0
4	EBS	0	1	0	0	0	0
5	NBS	0	1	0	0	0	0
6	PP	0	0	0	1	0	0
7	TI	0	0	0	1	0	0
8	TII	0	0	1	0	0	0
9	TVIII	1	0	0	0	0	0
10	GXT	0	0	0	1	0	0
11	SCH	0	0	0	0	1	0
12	HP	0	0	0	0	1	0
13	TC	0	0	0	0	0	1
14	HC	0	0	0	0	1	0
15	BC	0	0	0	0	1	0
16	BU	0	0	0	1	0	0
17	LTII	0	0	0	0	1	0
18	LHH	0	0	0	0	1	0
19	UC	0	0	0	0	0	1

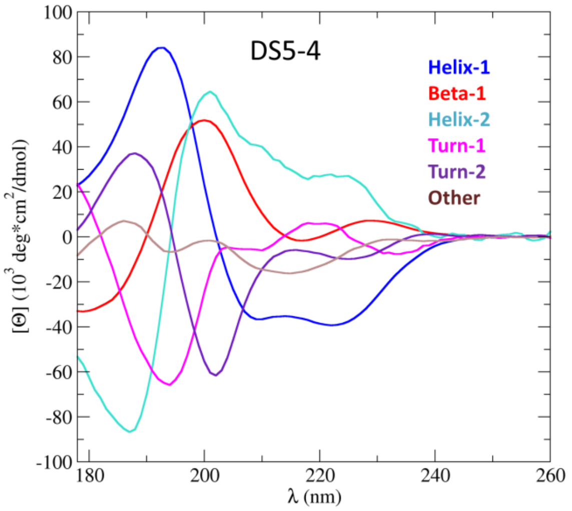

Figure S12: Assignment (left) and basis spectra (right) for the basis set DS5-4. Secondary structure elements for the assignment are abbreviated according to Table S5.

Map_DS6-1	i	1	2	3	4	5	6
k	α_{ki}	HEL1	HEL2	BST1	BST2	TRN1	COIL
1	3H	0	0	1	0	0	0
2	ALH	1	0	0	0	0	0
3	PIH	0	1	0	0	0	0
4	EBS	0	0	0	1	0	0
5	NBS	0	0	1	0	0	0
6	PP	0	1	0	0	0	0
7	TI	0	0	0	0	1	0
8	TII	0	0	0	0	0	1
9	TVIII	0	0	0	0	0	1
10	GXT	0	0	1	0	0	0
11	SCH	0	1	0	0	0	0
12	HP	0	0	0	1	0	0
13	TC	1	0	0	0	0	0
14	HC	1	0	0	0	0	0
15	BC	0	0	0	0	1	0
16	BU	0	0	0	0	1	0
17	LTII	0	0	0	0	1	0
18	LHH	1	0	0	0	0	0
19	UC	0	0	0	0	0	1

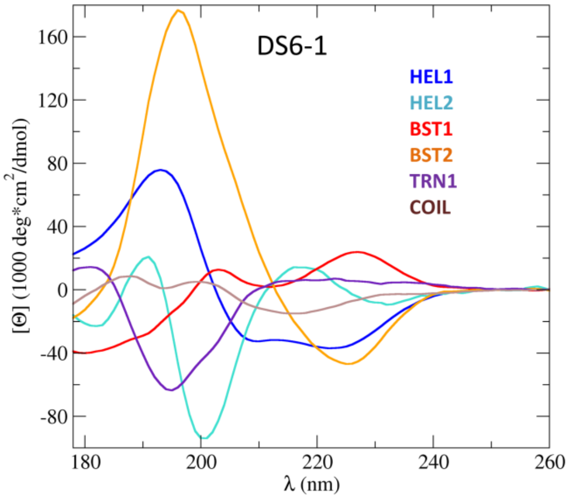

Figure S13: Assignment (left) and basis spectra (right) for the basis set DS6-1. Secondary structure elements for the assignment are abbreviated according to Table S5.

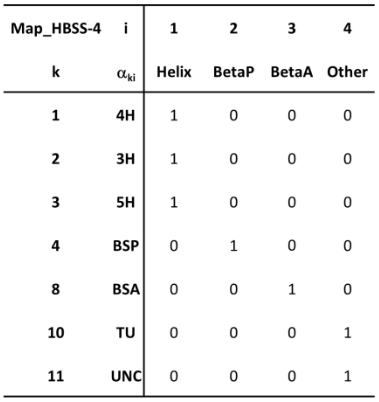

Map_HBSS-4	i	1	2	3	4
k	α_{ki}	Helix	BetaP	BetaA	Other
1	4H	1	0	0	0
2	3H	1	0	0	0
3	5H	1	0	0	0
4	BSP	0	1	0	0
8	BSA	0	0	1	0
10	TU	0	0	0	1
11	UNC	0	0	0	1

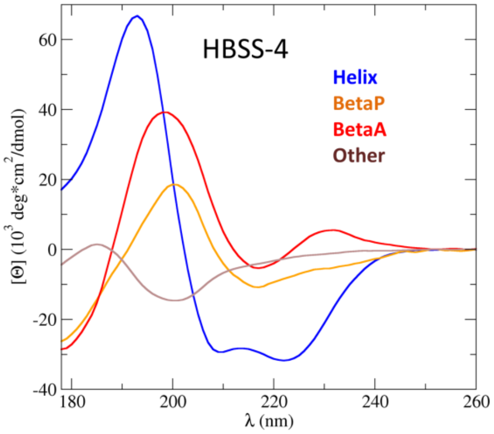

Figure S14: Assignment (left) and basis spectra (right) for the basis set HBSS-4. Secondary structure elements for the assignment are abbreviated according to Table S6.

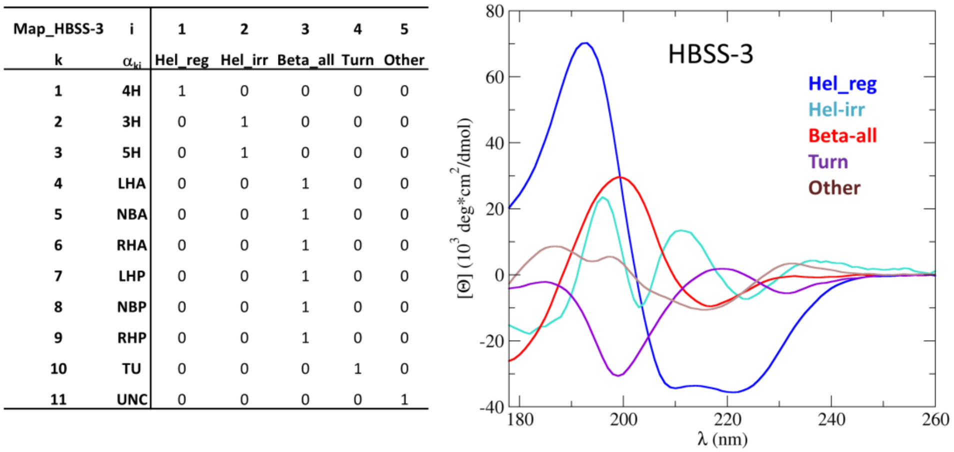

Map_HBSS-3	i	1	2	3	4	5
k	α_{ki}	Hel_reg	Hel_irr	Beta_all	Turn	Other
1	4H	1	0	0	0	0
2	3H	0	1	0	0	0
3	5H	0	1	0	0	0
4	LHA	0	0	1	0	0
5	NBA	0	0	1	0	0
6	RHA	0	0	1	0	0
7	LHP	0	0	1	0	0
8	NBP	0	0	1	0	0
9	RHP	0	0	1	0	0
10	TU	0	0	0	1	0
11	UNC	0	0	0	0	1

Figure S15: Assignment (left) and basis spectra (right) for the basis set HBSS-3. Secondary structure elements for the assignment are abbreviated according to Table S6.

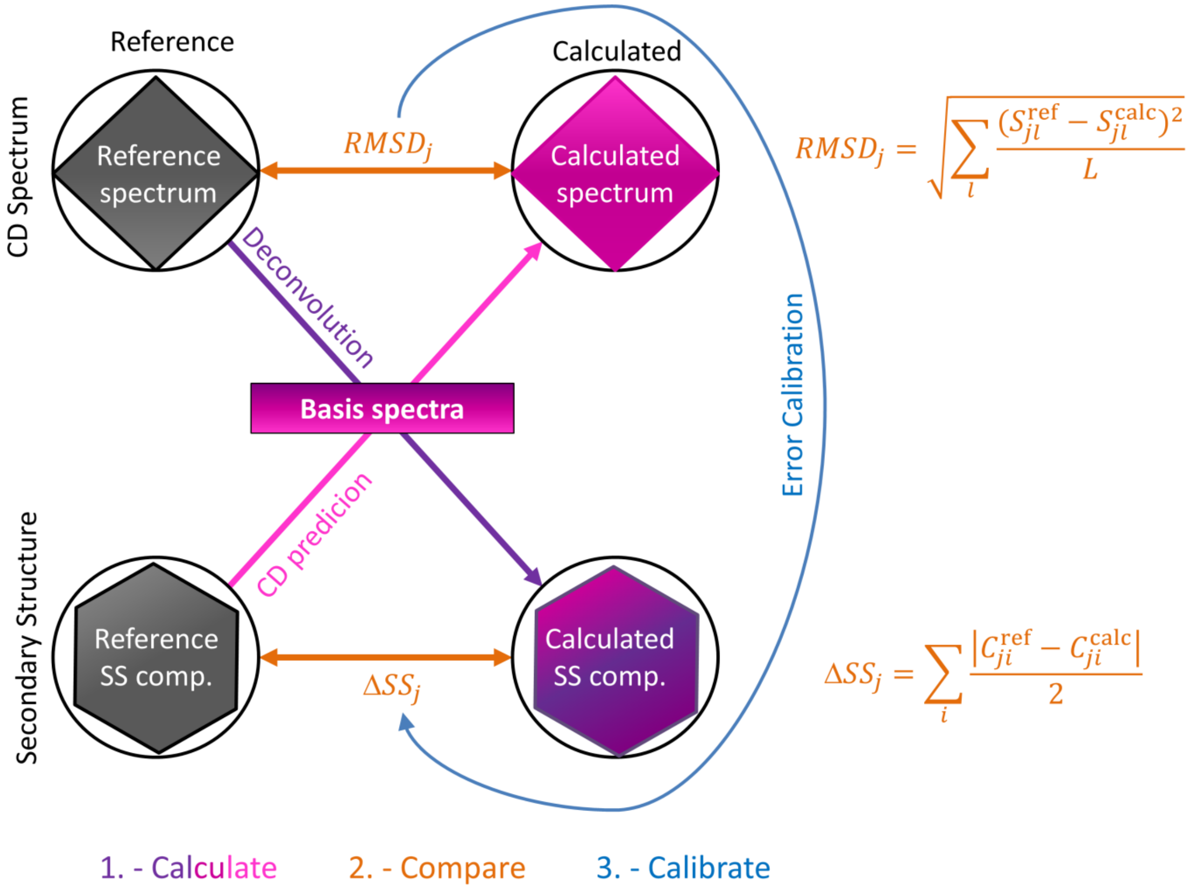

Figure S16: Calibration of the total model error. To estimate the error in the SS composition of structural models (ΔSS_j) based on the error of their predicted CD spectrum ($RMSD_j$), first CD spectra is predicted from the SS composition of reference structures, and ideal SS compositions are predicted (via deconvolution) from the available reference CD spectra for each protein j. Then, the reference spectra and SS compositions are compared to the predicted ones to obtain $RMSD_j$ vs. ΔSS_j pairs for each protein, which are fitted with an error model during an error calibration step (Section S8). The resulting error model can be used to estimate ΔSS_j from CD predictions using the same basis spectra.

BB_DS-dTSC3	i	1	2	3
k	α_{ki}	Alpha	Beta	Coil
1	3H	1	0	0
2	ALH	1	0	0
3	PIH	1	0	0
4	EBS	0	1	0
5	NBS	0	1	0
6	PP	0	0	1
7	TI	0	0	1
8	TII	0	0	1
9	TVIII	0	0	1
10	GXT	0	0	1
11	SCH	0	0	1
12	HP	0	0	1
13	TC	0	0	1
14	HC	0	0	1
15	BC	0	0	1
16	BU	0	0	1
17	LTII	0	0	1
18	LHH	0	0	1
19	UC	0	0	1

SC_DS-dTSC3	i	1	2	3	4
k	α_k	GRP1	GRP2	GRP3	GRP4
1	ALA	0	0	0	1
2	ASP	0	1	0	0
3	ASN	0	1	0	0
4	ARG	0	1	0	0
5	CYS	0	0	0	1
6	GLY	0	0	1	0
7	GLU	0	1	0	0
8	GLN	0	1	0	0
9	HIS	1	0	0	0
10	ILE	0	0	0	1
11	LEU	0	0	0	1
12	LYS	0	0	0	1
13	MET	0	0	0	1
14	PHE	1	0	0	0
15	PRO	0	0	0	1
16	SER	0	0	0	1
17	THR	0	0	0	1
18	TRP	1	0	0	0
19	TYR	1	0	0	0
20	VAL	0	0	0	1

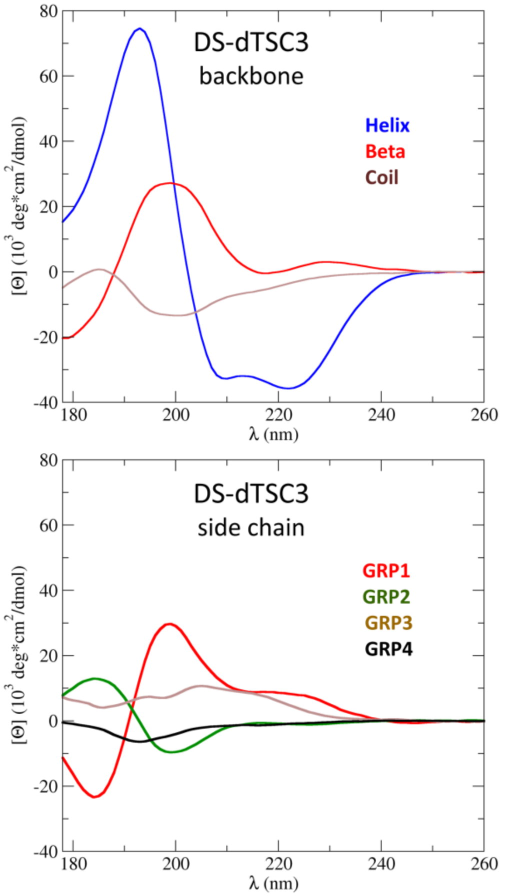

Figure S17: Assignment (left) and basis spectra (right) for the mixed basis set DS-dTSC3. The backbone and side-chain related basis spectra are shown on the top and bottom, respectively. Secondary structure elements for the assignment are abbreviated according to Table S5.

BB_DS6-1SC1	i	1	2	3	4	5	6
k	α_{ki}	Helix-1	Helix-2	Beta-1	Beta-2	Turn	Coil
1	3H	0	0	1	0	0	0
2	ALH	1	0	0	0	0	0
3	PIH	0	1	0	0	0	0
4	EBS	0	0	0	1	0	0
5	NBS	0	0	1	0	0	0
6	PP	0	1	0	0	0	0
7	TI	0	0	0	0	1	0
8	TII	0	0	0	0	0	1
9	TVIII	0	0	0	0	0	1
10	GXT	0	0	1	0	0	0
11	SCH	0	1	0	0	0	0
12	HP	0	0	0	1	0	0
13	TC	1	0	0	0	0	0
14	HC	1	0	0	0	0	0
15	BC	0	0	0	0	1	0
16	BU	0	0	0	0	1	0
17	LTII	0	0	0	0	1	0
18	LHH	1	0	0	0	0	0
19	UC	0	0	0	0	0	1

SC_DS6-1SC1	I	1	2	3	4	5	6
k	α_{ki}	GRP1	GRP2	GRP3	GRP4	GRP5	GRP6
1	ALA	0	0	0	0	1	0
2	ASP	1	0	0	0	0	0
3	ASN	0	0	1	0	0	0
4	ARG	0	0	0	0	0	1
5	CYS	0	1	0	0	0	0
6	GLY	0	0	0	0	0	1
7	GLU	0	0	1	0	0	0
8	GLN	0	0	0	1	0	0
9	HIS	0	0	0	1	0	0
10	ILE	0	0	1	0	0	0
11	LEU	0	0	0	0	1	0
12	LYS	0	0	0	1	0	0
13	MET	0	0	0	1	0	0
14	PHE	1	0	0	0	0	0
15	PRO	0	0	0	0	1	0
16	SER	0	0	1	0	0	0
17	THR	0	1	0	0	0	0
18	TRP	0	1	0	0	0	0
19	TYR	0	0	0	0	0	1
20	VAL	1	0	0	0	0	0

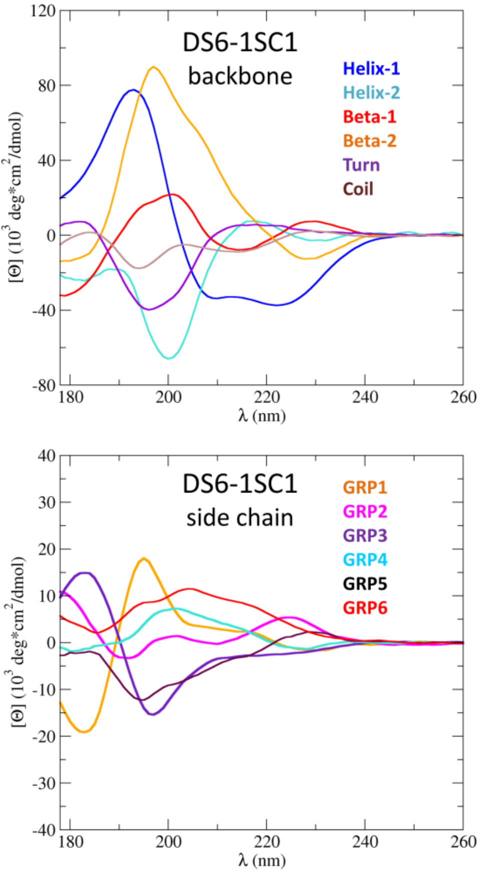

Figure S18: Assignment (left) and basis spectra (right) for the mixed basis set DS6-1SC1. The backbone and side-chain related basis spectra are shown on the top and bottom, respectively. Secondary structure elements for the assignment are abbreviated according to Table S5.

BB_DS5-4SC1	i	1	2	3	4	5	6
k	α_{ki}	Helix-1	Beta-1	Helix-2	Turn-1	Turn-2	Other
1	3H	0	0	1	0	0	0
2	ALH	1	0	0	0	0	0
3	PIH	0	0	0	0	1	0
4	EBS	0	1	0	0	0	0
5	NBS	0	1	0	0	0	0
6	PP	0	0	0	1	0	0
7	TI	0	0	0	1	0	0
8	TII	0	0	1	0	0	0
9	TVIII	1	0	0	0	0	0
10	GXT	0	0	0	1	0	0
11	SCH	0	0	0	0	1	0
12	HP	0	0	0	0	1	0
13	TC	0	0	0	0	0	1
14	HC	0	0	0	0	1	0
15	BC	0	0	0	0	1	0
16	BU	0	0	0	1	0	0
17	LTII	0	0	0	0	1	0
18	LHH	0	0	0	0	1	0
19	UC	0	0	0	0	0	1

SC_DS5-4SC1	i	1	2	3	4	5	6
k	α_{ki}	GRP1	GRP2	GRP3	GRP4	GRP5	GRP6
1	ALA	0	0	0	0	1	0
2	ASP	0	0	0	1	0	0
3	ASN	0	0	0	0	1	0
4	ARG	1	0	0	0	0	0
5	CYS	0	0	0	1	0	0
6	GLY	0	0	0	0	0	1
7	GLU	0	0	1	0	0	0
8	GLN	0	0	0	1	0	0
9	HIS	0	1	0	0	0	0
10	ILE	1	0	0	0	0	0
11	LEU	0	0	1	0	0	0
12	LYS	0	0	0	0	0	1
13	MET	0	0	0	0	0	1
14	PHE	0	1	0	0	0	0
15	PRO	0	0	0	0	1	0
16	SER	1	0	0	0	0	0
17	THR	0	0	0	0	1	0
18	TRP	1	0	0	0	0	0
19	TYR	0	1	0	0	0	0
20	VAL	0	0	0	0	0	1

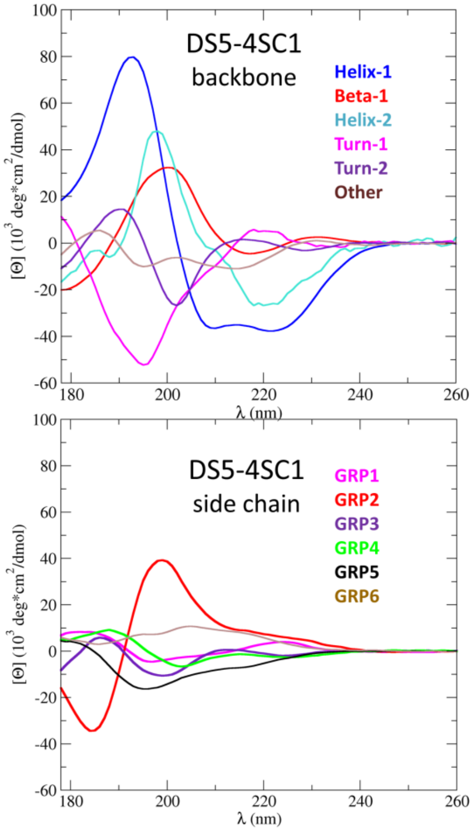

Figure S19: Assignment (left) and basis spectra (right) for the mixed basis set DS5-4SC1. The backbone and side-chain related basis spectra are shown on the top and bottom, respectively. Secondary structure elements for the assignment are abbreviated according to Table S5.

BB_DSSP-1SC3	i	1	2	3	4
k	α_{ki}	Helix	Sheet	Bridge	Other
1	3H	1	0	0	0
2	4H	1	0	0	0
3	5H	0	1	0	0
4	BS	0	1	0	0
5	BB	0	0	1	0
6	TU	0	0	0	1
7	BE	0	0	0	1
8	UC	0	0	0	1

SC_DSSP-1SC3	i	1	2	3	4	5	6
k	α_{ki}	GRP1	GRP2	GRP3	GRP4	GRP5	GRP6
1	ALA	0	0	0	0	1	0
2	ASP	0	0	0	0	0	1
3	ASN	0	0	0	1	0	0
4	ARG	0	0	0	1	0	0
5	CYS	1	0	0	0	0	0
6	GLY	0	0	0	0	1	0
7	GLU	1	0	0	0	0	0
8	GLN	1	0	0	0	0	0
9	HIS	0	0	0	0	1	0
10	ILE	0	1	0	0	0	0
11	LEU	0	0	0	0	0	1
12	LYS	0	0	0	0	0	1
13	MET	0	0	0	0	0	1
14	PHE	0	0	0	0	1	0
15	PRO	0	0	1	0	0	0
16	SER	0	0	0	0	1	0
17	THR	0	0	1	0	0	0
18	TRP	0	0	0	1	0	0
19	TYR	0	0	1	0	0	0
20	VAL	0	0	0	1	0	0

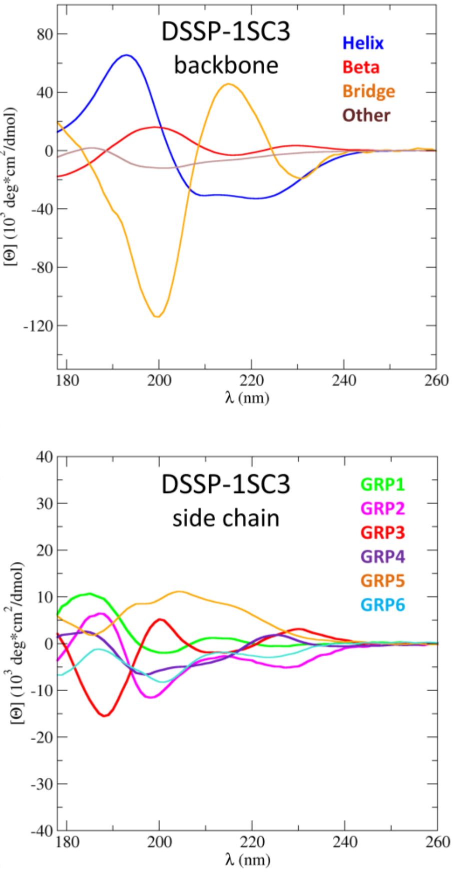

Figure S20: Assignment (left) and basis spectra (right) for the mixed basis set DSSP-1SC3. The backbone and side-chain related basis spectra are shown on the top and bottom, respectively. Secondary structure elements for the assignment are abbreviated according to Table S4.

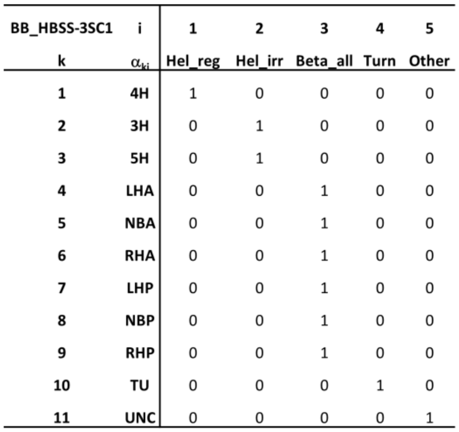

BB_HBSS-3SC1	i	1	2	3	4	5
k	α_{ki}	Hel_reg	Hel_irr	Beta_all	Turn	Other
1	4H	1	0	0	0	0
2	3H	0	1	0	0	0
3	5H	0	1	0	0	0
4	LHA	0	0	1	0	0
5	NBA	0	0	1	0	0
6	RHA	0	0	1	0	0
7	LHP	0	0	1	0	0
8	NBP	0	0	1	0	0
9	RHP	0	0	1	0	0
10	TU	0	0	0	1	0
11	UNC	0	0	0	0	1

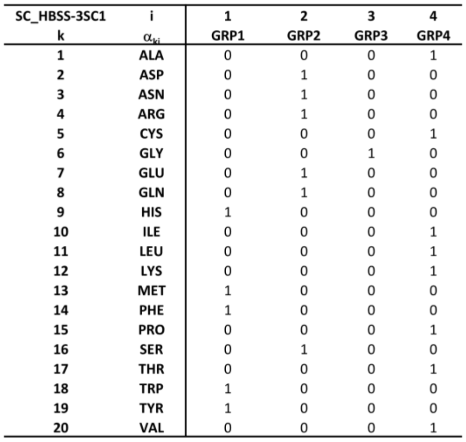

SC_HBSS-3SC1	i	1	2	3	4
k	α_{ki}	GRP1	GRP2	GRP3	GRP4
1	ALA	0	0	0	1
2	ASP	0	1	0	0
3	ASN	0	1	0	0
4	ARG	0	1	0	0
5	CYS	0	0	0	1
6	GLY	0	0	1	0
7	GLU	0	1	0	0
8	GLN	0	1	0	0
9	HIS	1	0	0	0
10	ILE	0	0	0	1
11	LEU	0	0	0	1
12	LYS	0	0	0	1
13	MET	1	0	0	0
14	PHE	1	0	0	0
15	PRO	0	0	0	1
16	SER	0	1	0	0
17	THR	0	0	0	1
18	TRP	1	0	0	0
19	TYR	1	0	0	0
20	VAL	0	0	0	1

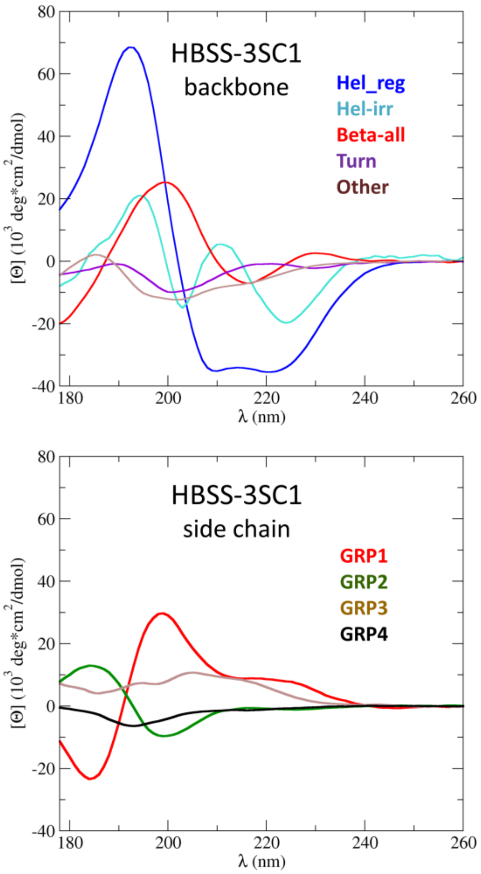

Figure S21: Assignment (left) and basis spectra (right) for the mixed basis set HBSS-3SC1. The backbone and side-chain related basis spectra are shown on the top and bottom, respectively. Secondary structure elements for the assignment are abbreviated according to Table S6.

BB_HBSS-3SCF	i	1	2	3	4	5
k	α_{ki}	Hel-reg	Hel-irr	Beta-all	Turn	Other
1	4H	1	0	0	0	0
2	3H	0	1	0	0	0
3	5H	0	1	0	0	0
4	LHA	0	0	1	0	0
5	NBA	0	0	1	0	0
6	RHA	0	0	1	0	0
7	LHP	0	0	1	0	0
8	NBP	0	0	1	0	0
9	RHP	0	0	1	0	0
10	TU	0	0	0	1	0
11	UNC	0	0	0	0	1

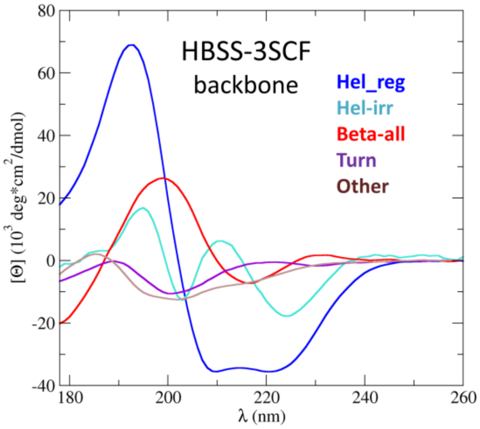

SC_HBSS-3SCF (Basis spectra abbreviated by 1-letter AA codes)

	l	1	2	3	4	5	6	7	8	9	10	11	12	13	14	15	16	17	18	19	20
k	α_{ki}	A	D	N	R	C	G	E	Q	H	I	L	K	M	F	P	S	T	W	Y	V
1	ALA	1	0	0	0	0	0	0	0	0	0	0	0	0	0	0	0	0	0	0	0
2	ASP	0	1	0	0	0	0	0	0	0	0	0	0	0	0	0	0	0	0	0	0
3	ASN	0	0	1	0	0	0	0	0	0	0	0	0	0	0	0	0	0	0	0	0
4	ARG	0	0	0	1	0	0	0	0	0	0	0	0	0	0	0	0	0	0	0	0
5	CYS	0	0	0	0	1	0	0	0	0	0	0	0	0	0	0	0	0	0	0	0
6	GLY	0	0	0	0	0	1	0	0	0	0	0	0	0	0	0	0	0	0	0	0
7	GLU	0	0	0	0	0	0	1	0	0	0	0	0	0	0	0	0	0	0	0	0
8	GLN	0	0	0	0	0	0	0	1	0	0	0	0	0	0	0	0	0	0	0	0
9	HIS	0	0	0	0	0	0	0	0	1	0	0	0	0	0	0	0	0	0	0	0
10	ILE	0	0	0	0	0	0	0	0	0	1	0	0	0	0	0	0	0	0	0	0
11	LEU	0	0	0	0	0	0	0	0	0	0	1	0	0	0	0	0	0	0	0	0
12	LYS	0	0	0	0	0	0	0	0	0	0	0	1	0	0	0	0	0	0	0	0
13	MET	0	0	0	0	0	0	0	0	0	0	0	0	1	0	0	0	0	0	0	0
14	PHE	0	0	0	0	0	0	0	0	0	0	0	0	0	1	0	0	0	0	0	0
15	PRO	0	0	0	0	0	0	0	0	0	0	0	0	0	0	1	0	0	0	0	0
16	SER	0	0	0	0	0	0	0	0	0	0	0	0	0	0	0	1	0	0	0	0
17	THR	0	0	0	0	0	0	0	0	0	0	0	0	0	0	0	0	1	0	0	0
18	TRP	0	0	0	0	0	0	0	0	0	0	0	0	0	0	0	0	0	1	0	0
19	TYR	0	0	0	0	0	0	0	0	0	0	0	0	0	0	0	0	0	0	1	0
20	VAL	0	0	0	0	0	0	0	0	0	0	0	0	0	0	0	0	0	0	0	1

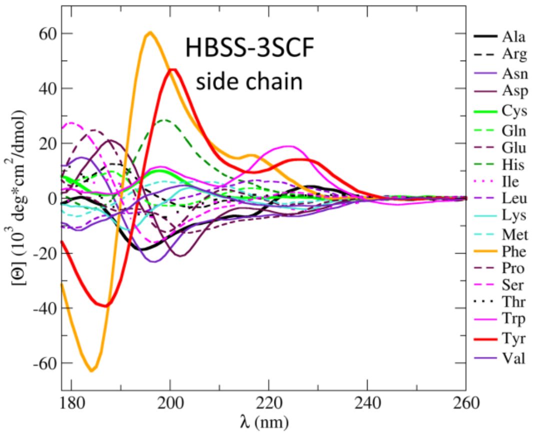

Figure S22: Assignment (left) and basis spectra (right) for the mixed basis set HBSS-3SCF. The backbone and side-chain related basis spectra are shown on the top and bottom, respectively. Secondary structure elements for the assignment are abbreviated according to Table S6.

Set_Sreer-1	i	1	2	3	4	5	6
k	α_k	Hel-reg	Hel-irr	Beta-reg	Bet-irr	Turn	Unord.
1	3H	0	1	0	0	0	0
2	ALH	1	0	0	0	0	0
3	PIH	1	0	0	0	0	0
4	EBS	0	0	1	0	0	0
5	NBS	0	0	1	0	0	0
6	PP	0	0	0	0	0	1
7	TI	0	1	0	0	0	0
8	TII	0	0	0	0	1	0
9	TVIII	0	0	0	0	1	0
10	GXT	0	0	0	0	1	0
11	SCH	0	1	0	0	0	0
12	HP	0	0	0	1	0	0
13	TC	0	0	0	0	1	0
14	HC	0	1	0	0	0	0
15	BC	0	0	0	1	0	0
16	BU	0	0	0	1	0	0
17	LTII	0	0	0	0	1	0
18	LHH	0	0	0	0	1	0
19	UC	0	0	0	0	0	1

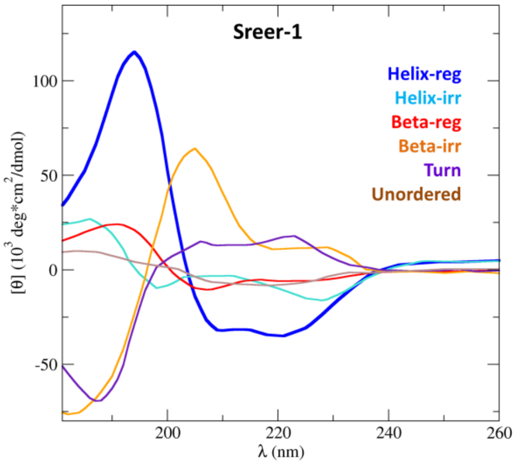

Figure S23: Assignment (left) and basis spectra (right) for the adapted basis set Sreer-1. Secondary structure elements for the assignment are abbreviated according to Table S5.

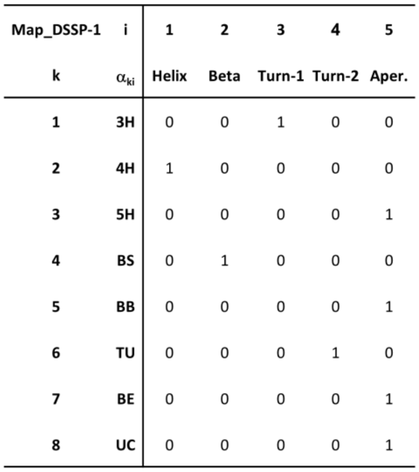

Map_DSSP-1	i	1	2	3	4	5
k	α_{ki}	Helix	Beta	Turn-1	Turn-2	Aper.
1	3H	0	0	1	0	0
2	4H	1	0	0	0	0
3	5H	0	0	0	0	1
4	BS	0	1	0	0	0
5	BB	0	0	0	0	1
6	TU	0	0	0	1	0
7	BE	0	0	0	0	1
8	UC	0	0	0	0	1

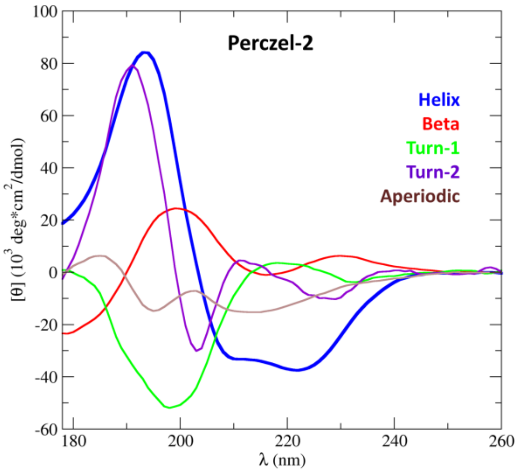

Figure S24: Assignment (left) and basis spectra (right) for the adapted basis set Preczel-2. Secondary structure elements for the assignment are abbreviated according to Table S4.

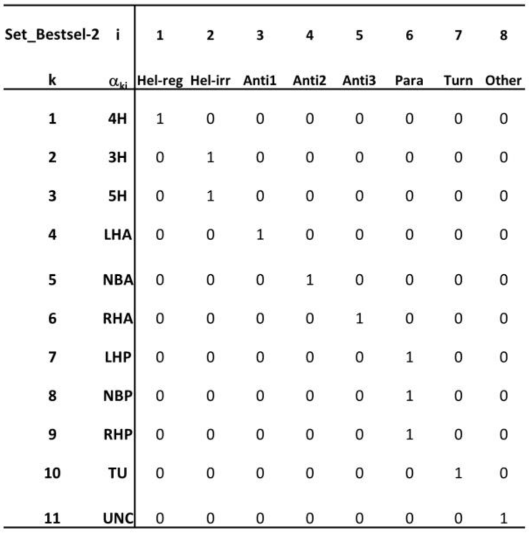

Set_Bestsel-2	i	1	2	3	4	5	6	7	8
k	α_{ki}	Hel-reg	Hel-irr	Anti1	Anti2	Anti3	Para	Turn	Other
1	4H	1	0	0	0	0	0	0	0
2	3H	0	1	0	0	0	0	0	0
3	5H	0	1	0	0	0	0	0	0
4	LHA	0	0	1	0	0	0	0	0
5	NBA	0	0	0	1	0	0	0	0
6	RHA	0	0	0	0	1	0	0	0
7	LHP	0	0	0	0	0	1	0	0
8	NBP	0	0	0	0	0	1	0	0
9	RHP	0	0	0	0	0	1	0	0
10	TU	0	0	0	0	0	0	1	0
11	UNC	0	0	0	0	0	0	0	1

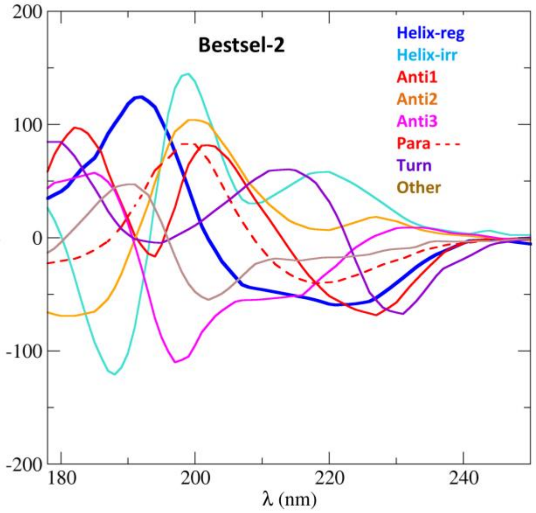

Figure S25: Assignment (left) and basis spectra (right) for the adapted basis set Bestsel-2. Derived previously by Micsonai *et al.* [3] Secondary structure elements for the assignment are abbreviated according to Table S6.

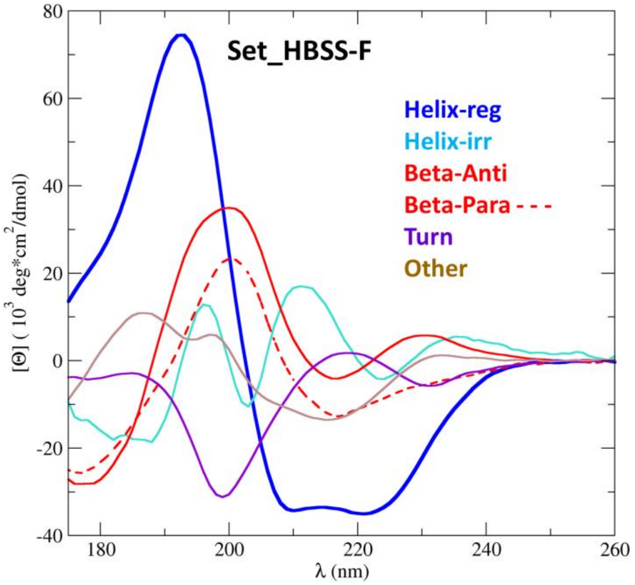

Figure S26: Derived initial basis spectra for the structure classification HbSS, basic classification library.

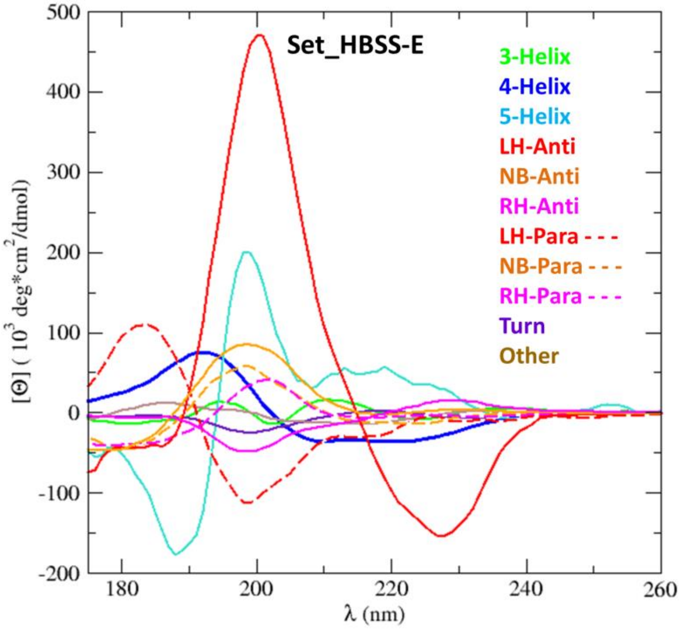

Figure S27: Derived initial basis spectra for the structure classification algorithm HbSS, extended library (HbSS_ext).

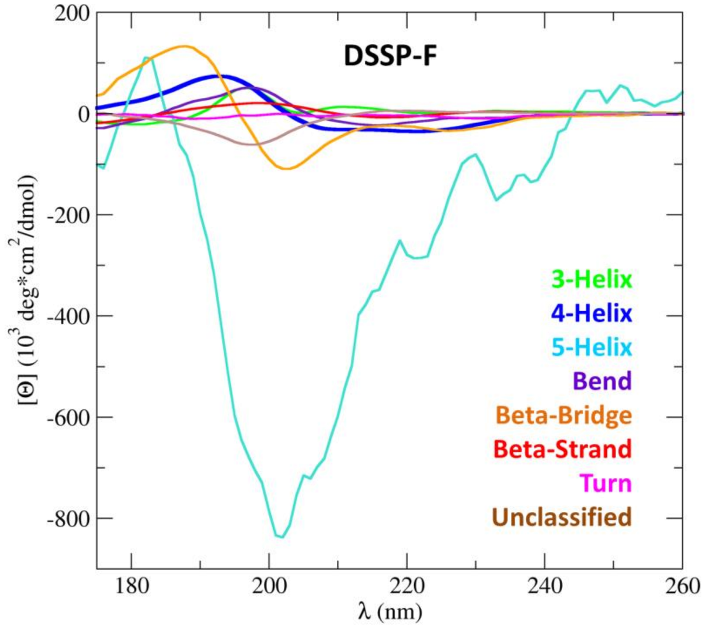

Figure S28: Derived initial basis spectra for the structure classification DSSP.

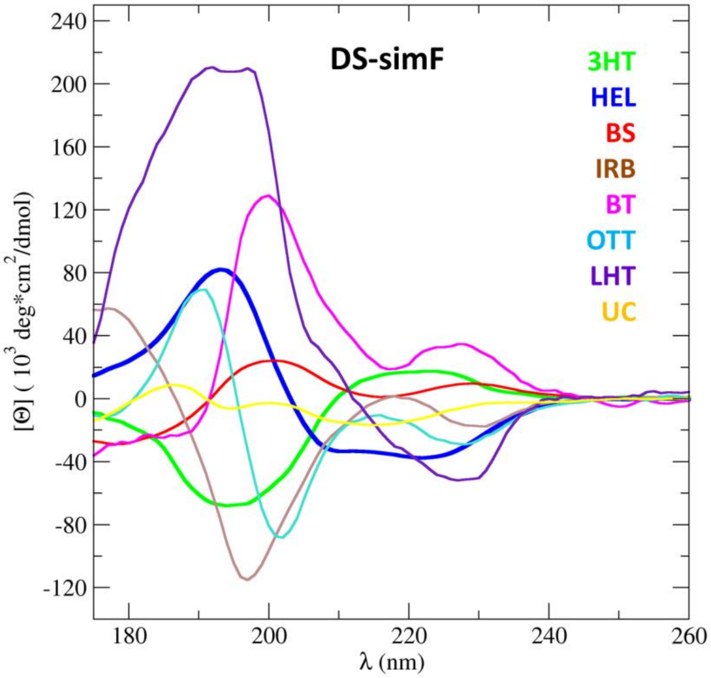

Figure S29: Derived initial basis spectra for the structure classification DISICL, simplified classification library (DS_sim).

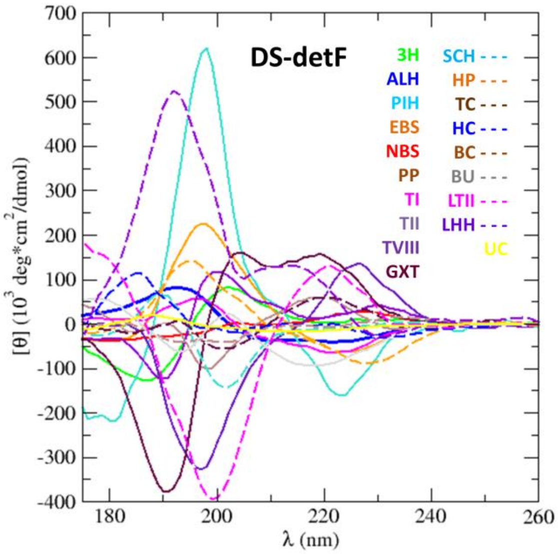

Figure S30: Derived initial basis spectra for the structure classification DISICL, detailed classification library (DS_det).

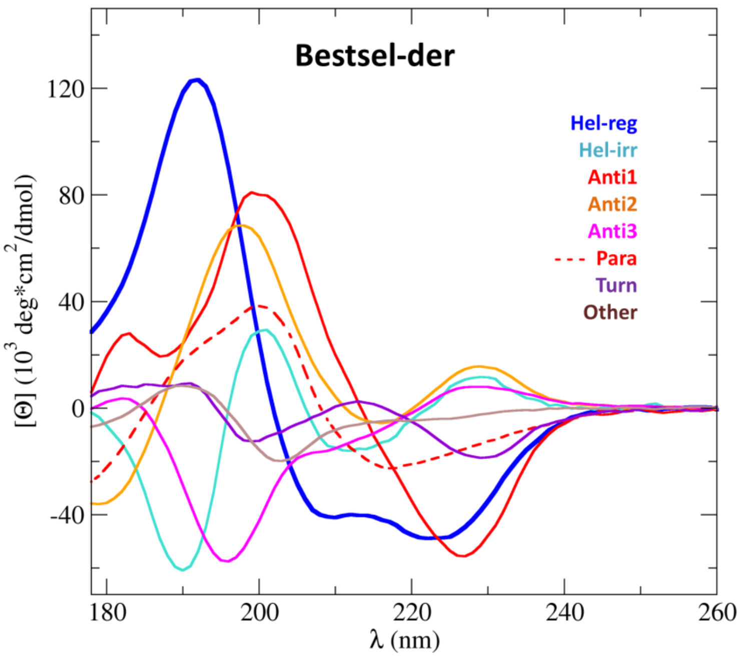

Figure S31: derived basis spectra for the Bestsel_der basis set. This basis set was derived from the measured CD spectra and estimated secondary structure compositions of the SP175 set, as predicted by the BeStSel deconvolution algorithm. Note that BeStSel estimates were obtained using the BeStSel web application (bestsel.elte.hu) by uploading the SP175 and TS8 CD spectra, and fitting basis spectra to the 175-250 nm wavelength range.

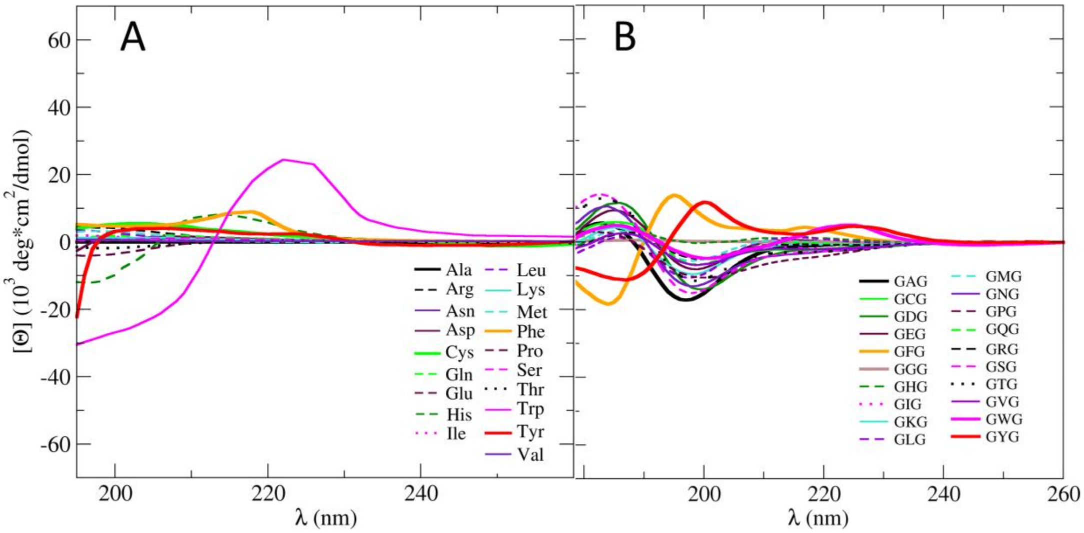

Figure S32: Comparison between the CD spectra of A) isolated natural amino acids and B) of Ac-GXG-NH2 peptides (X being any amino acid)..

References:

(1) Sreerama, N.; Woody, R. W. Poly (Pro) II Helixes in Globular Proteins: Identification and Circular Dichroic Analysis. *Biochemistry* **1994**, *33* (33), 10022–10025.

(2) Perczel, Andras; Hollósi, M.; Tudnady, G.; Fasman, G. D. Convex Constraint Analysis: A Natural Deconvolution of Circular Dichroism Curves of Proteins. *Protein Engineering* **1991**, *4* (6), 669–679.

(3) Micsonai, A.; Wien, F.; Kernya, L.; Lee, Y.-H.; Goto, Y.; Réfrégiers, M.; Kardos, J. Accurate Secondary Structure Prediction and Fold Recognition for Circular Dichroism Spectroscopy. *Proceedings of the National Academy of Sciences* **2015**, *112* (24), E3095–E3103. https://doi.org/10.1073/pnas.1500851112.

(4) Gao, F.; Han, L. Implementing the Nelder-Mead Simplex Algorithm with Adaptive Parameters. *Computational Optimization and Applications* **2012**, *51* (1), 259–277. https://doi.org/10.1007/s10589-010-9329-3.

(5) Boggs, P. T.; Rogers, J. E. Orthogonal Distance Regression. *NISTIR 89–4197* **2009**, 1–14.

(6) Nishino, H.; Kosaka, A.; Hembury, G. A.; Matsushima, K.; Inoue, Y. The pH Dependence of the Anisotropy Factors of Essential Amino Acids. *Journal of the Chemical Society, Perkin Transactions 2* **2002**, No. 3, 582–590. https://doi.org/10.1039/b108575c.

(7) Reed, J.; Reed, T. A. A Set of Constructed Type Spectra for the Practical Estimation of Peptide Secondary Structure from Circular Dichroism. *Anal. Biochem.* **1997**, *254*, 36–40.

(8) Oakley, M. T.; Bulheller, B. M.; Hirst, J. D. First-Principles Calculations of Protein Circular Dichroism in the Far-Ultraviolet and Beyond. *Chirality* **2006**, *18*, 340–347. https://doi.org/10.1002/chir.20264.

(9) Louis-Jeune, C.; Andrade-Navarro, M. A.; Perez-Iratxeta, C. Prediction of Protein Secondary Structure from Circular Dichroism Using Theoretically Derived Spectra. *Proteins: Structure, Function, and Bioinformatics* **2012**, *80* (2), 374–381. https://doi.org/10.1002/prot.23188.

(10) Shen, Y.; Bax, A. SPARTA+: A Modest Improvement in Empirical NMR Chemical Shift Prediction by Means of an Artificial Neural Network. *Journal of Biomolecular NMR* **2010**, *48* (1), 13–22. https://doi.org/10.1007/s10858-010-9433-9.

(11) Lees, J. G.; Miles, A. J.; Wien, F.; Wallace, B. A. A Reference Database for Circular Dichroism Spectroscopy Covering Fold and Secondary Structure Space. *Bioinformatics* **2006**, *22* (16), 1955–1962. https://doi.org/10.1093/bioinformatics/btl327.

(12) Kabsch, W.; Sander, C. Dictionary of Protein Secondary Structure: Pattern Recognition of Hydrogen-Bonded and Geometrical Features. *Biopolymers* **1983**, *22* (12), 2577–2637.

(13) Nagy, G.; Oostenbrink, C. Dihedral-Based Segment Identification and Classification of Biopolymers I: Proteins. *J. Chem Inf. Model.* **2014**, *54* (1), 266–277. https://doi.org/10.1021/ci400541d.

(14) Mavridis, L.; Janes, R. W. PDB2CD: A Web-Based Application for the Generation of Circular Dichroism Spectra from Protein Atomic Coordinates. *Bioinformatics* **2017**, *33* (1), 56–63. https://doi.org/10.1093/bioinformatics/btw554.